Marine And Petroleum Geology
July 2023, Volume 153 Pages 106273 (20p.)
https://doi.org/10.1016/j.marpetgeo.2023.106273
https://archimer.ifremer.fr/doc/00834/94641/

Plumbing systems and associated seafloor fluid seepages in deep-water Nigeria: Factors controlling their architecture and cyclic evolution

Marsset Tania [1, *], Pape T. [2], Simplet Laure [1], Dennielou Bernard [1], Ruffine Livio [1], Bohrmann G. [2], Révillon Sidonie [3]

[1] Geo-Ocean, Univ Brest, CNRS, Ifremer, UMR6538, F-29280, Plouzane, France
[2] MARUM – Center for Marine Environmental Sciences and Faculty of Geosciences, University of Bremen, Klagenfurter Strasse 4, 28359, Bremen, Germany
[3] SEDISOR, LGO – IUEM, Place N. Copernic, 29280, Brest, France

* Corresponding author : Tania Marsset, email address : tania.marsset@ifremer.fr

Abstract :

A range of plumbing systems has been identified in deep-water Nigeria by interpreting multi-scale seismic data sets (reprocessed 3D exploration seismic reflection data and 2D very high-resolution near-bottom seismic reflection data) as well as sedimentological and geochemical data obtained from a long sediment core recovered by the seafloor drill rig MARUM-MeBo70. The plumbing systems are characterized by diverse fault networks and lie above tectonic features including thrust/fold structures and strike-slip faults linked to gravity-driven deformation caused by underlying over-pressured shales. The plumbing systems are associated with fluid seeping structures at the seafloor such as pockmarks, mud volcanoes and seafloor zonations colonized by living benthic macrofauna typical of active fluid flow. The comparison of seismic stratigraphic sequences with climate and environmental proxies determined for sediments including lithology, element ratios such as Ca/Fe and Zr/Rb, sedimentation rates, and planktonic foraminifera δ18O records shows a control of short-term (0.1–0.4 Myr) and long-term (around 1 Myr) sedimentary cycles. During short-term fluctuations, the recurrence of fluid seeping structures is controlled by the lithology (coarse-grained versus fine-grained sediments) linked to glacial-interglacial fluctuations and a monsoon regime. Conditions favorable for fluid flow are related to the deposition of coarse-grained layers, glacial periods, sea-level lowstands, and low sedimentation rates. We hypothesize that cyclic gravity-driven sediment deformations controlled by glacial-interglacial and long-term variations in accommodation and sedimentation, have led to the cyclic evolution of the plumbing systems and associated seeping structures since the Plio-Pleistocene.

Highlight

► Diverse faults networks are associated with varied fluid flow structures. ► The recurrence of fluid flow structures is coeval to glacial periods. ► Gravity-driven deformations possibly control fluid flow during the Pleistocene.

Keywords : Niger Delta, Pockmarks, Mud volcano, Climate, Eustasy, Gravity-driven deformation, Depositional sequences

1. Introduction

Submarine cold seep systems comprise three elements: (i) a source layer of the fluid of varied composition such as microbial or thermogenic gas, pore water, fresh water or oil, (ii) a plumbing system (transitory section from the source layer to seabed features), such as faults or pipes, which promotes fluid migration, and (iii) seafloor features indicative of fluid venting (high fluxes) or seeping (low fluxes), such as mud volcanoes, pockmarks, carbonate mounds or gas hydrate pingos (Milkov, 2000; Bailey et al., 2003; Berndt et al., 2003; Gay et al., 2007; 2017; Hovland et al., 2010; Andresen and Huuse, 2011; Talukder, 2012; Dumke et al., 2014; Foschi and Cartwright, 2016; Paganoni et al., 2018). Submarine cold seep systems have implications for subseabed and seabed geological features, and the biological marine environment (Judd and Hovland, 2009; Suess, 2014). Understanding their potential for fluid leakage has important consequences for geological resources (e.g., hydrocarbon and water), CO_2 storage and geohazards (e.g., sedimentary instabilities) (Graue, 2000; Heggland, 2003; Maestrelli et al., 2017). Recently, submarine cold seep systems have gained significant interest as they are a source of methane escape into the ocean, potentially reaching the atmosphere and acting as a potent greenhouse gas (Shakhova et al., 2014; Portnov et al., 2016; Andreassen et al., 2017; Etiope et al., 2019; Stott et al., 2019; Dean, 2020; Foschi et al., 2020).

Factors known to precondition and destabilize pore pressure equilibrium, resulting in seafloor fluid expulsion and the formation of cold seeps, are:

i) Sea-level changes (Plaza-Faverola et al., 2011; Niyazi et al., 2022). Sea-level drops cause a reduction in hydrostatic pore pressure in fluid reservoirs that lowers gas solubility and results in gas exsolution. Gas accumulates preferentially in porous (i.e., sand-bearing) layers sealed by less permeable (i.e., sand-poor) layers generating overpressure. Fluid expulsion occurs when overpresure is high enough to breach the seal (Magara, 1978; Bolton et al., 1998; Dugan et al., 2003; Lafuerza et al., 2009).

ii) High sedimentation rates and tectonic loading. On active and passive margins, overpressure forces the fluid upwards, facilitated by rock and/or sedimentary layers deformation (Milkov, 2000; Dewangan et al., 2010; Sun et al., 2013; Chenrai and Huuse, 2017; Waage and al., 2019; Ma et al. 2021). High sedimentation rates and low permeability of sediments tend to inhibit the expulsion of pore water during compaction and create potential source layers upward fluid injections (Osborne and Swarbrick, 1997; Maltman and Bolton, 2003).

iii) Formation and destabilization of gas hydrates. Gas and water permeability in sediments is reduced when a large fraction of pore space is occupied by gas hydrates (Nimblett and Ruppel, 2003; Bangs et al., 2011). Pressure build-up can appear beneath the base of the Gas Hydrate Stability Zone (GHSZ) until high gas pressure forces the gas to migrate through the GHSZ to seafloor vents (Trehu et al., 2004; Plaza-Faverola et al., 2017). Gas hydrate dissociation and dissolution occur when the system is not at thermal and/or pressure steady-state. Changes in stability of hydrostatic pressure and temperature can be caused by rapid climatic and sea-level changes (Kennett et al., 2000; Phrampus and Hornbach, 2012; Darnell and Flemings, 2015; Mazzini et al., 2017; Serov et al., 2017; Feng et al., 2018) or changes in salinity (Riboulot et al., 2018). Gas hydrate dissociation and dissolution can generate overpressure and initiate hydrofracturing of overlying sedimentary layers leading to seepage (Xu and Germanovitch, 2006). Other factors affecting gas hydrate dynamics are high sedimentation rates, slope instability and flux and/or concentration of methane at the GHSZ (Cathles et al., 2010; Bohrmann and Torres, 2014; Sultan et al., 2014). Based on the results of a modeling case study, sedimentation-induced hydrate recycling was proposed, including a phase of free gas breakthrough and migration into the GHSZ, followed by the formation of a new hydrate layer (Schmidt et al., 2022).

iv) Mineralogical and geochemical sediment composition and mechanical properties linked to parameters such as the distribution of pore water constituents and gas hydrates (Lafuerza et al., 2009; Pennino et al., 2014; Sultan et al., 2016; Taleb et al., 2020).

v) Microbial processes such as consumption of organic matter generate escape of microbial gas (e.g., Berndt, 2005; Wallmann et al., 2006; Karaket et al., 2021).

Areas where the three elements of submarine cold seep systems are known and where the controlling factors have been distinguished remain poorly documented, particularly in complex tectonic settings.The main objective of this study is to present new information on the architecture and evolution of submarine cold seep systems and the controlling factors. Accordingly, we investigated the offshore Plio-Pleistocene eastern Niger Delta (Gulf of Guinea, West African margin) in a compressive tectonic setting (Fig. 1). It encompasses a pockmark field, an isolated mud volcano, an area with slope failures, and an area with living benthic macrofauna indicative of seafloor fluid escape. These characteristics make this region ideal to study cold seep systems and their forcing factors.

Our findings provide new insights into the role of climate/eustasy and gravity-driven deformation at glacial-interglacial time scales on fluid migration in offshore deltas located in the Equatorial domain.

2. Geological background and previous work

2.1 Tectonic-sedimentary setting and fluid-related features in the Niger Delta

The 12- km- thick Niger Delta (Gulf of Guinea) (Fig. 1A to 1C) spread out over the West African margin from Early Cretaceous times at the junction of tri-rift systems in relation to the opening of the South Atlantic Ocean (Burke et al., 1971; Burke, 1972; Lehner and De Ruiter, 1977). Three seaward prograding formations have been identified in the depositional belts of the margin (Fig. 1D): (1) the Akata formation mainly comprises thick shale sequences (potential fluid source rock) and turbiditic sands (potential reservoirs in deep-water areas) deposited from Paleocene to Recent during sea-level lowstands; (2) the Agbada formation consists mainly of paralic siliciclastics, i.e*.,* mainly deltaic sediments (major petroleum-

bearing unit) deposited from Late Eocene to Recent; (3) the Benin formation comprises fluvial sands (poor reservoir quality) deposited from latest Eocene to Recent (Short and Stauble, 1967; Burke, 1972; Evamy et al., 1978; Whiteman, 1982; Doust and Omatsola, 1990; Tuttle et al., 1999).

During the Plio-Pleistocene, the stacking patterns comprised imbricated long-duration (around 1 Myr) and short-duration (around 0.1-0.4 Myr) stratigraphic sequences that are marked by a prograding/retrograding sedimentary pattern (Jermannaud et al., 2010; Riboulot et al., 2012; Chima et al., 2020). The increase in sedimentation rates in the Gulf of Guinea during the Quaternary is attributed to the West African Monsoon, which supplies precipitation in the Niger watershed and controls riverine runoff, vegetation cover, the rate and type of erosion (mechanical or chemical), and the transport capacity of rivers (Weldeab et al., 2011; Collins et al., 2014; Govin et al., 2014; Lézine et al., 2014; Armitage et al., 2015). Monsoon precipitations are driven by the insolation linked to 23 ka precession cycles but is also highly dependent on the development of high-latitude polar icecaps tuned to 100 ka eccentricity cycles (Zabel et al., 2001; Caley et al., 2011; Weldeab et al., 2011).

During progradation of the Niger Delta, gravity-driven sediment deformation formed a series of extensional, transitional and compressional tectonic domains (Damuth, 1994; Morley and Guerin, 1996; Wu and Bally, 2000; Fig. 1C). Margin structuration was initiated by the development of overpressured layers in the Akata shales coincident with detachment faults, and gravity tectonism was caused by shale mobility (Knox and Omatsola, 1989; Doust and Omatsola, 1990; Briggs et al., 2006). At each of the depositional belts, gravity tectonism is expressed by complex structures, including deformed shale bodies, roll-over anticlines, and collapsed growth-fault crests (Evamy et al., 1978; Xiao and Suppe, 1992) (Fig. 1B and 1C). This pattern of deposition of the Niger Delta has continued until present (Armentrout et. al., 2000; Hooper et al., 2002; Bellingham et. al., 2014).

Corredor et al. (2005) proposed to subdivide the offshore part of the Niger Delta into five major structural provinces (Fig. 1E): (1) an extensional province, (2) a mobile shale ("mud-diapirs") province, (3) an inner fold-and-thrust belt, (4) a transitional detachment fold province

characterized by little or no deformation interspersed with large detachment folds, and (5) an outer fold-and-thrust belt. The distal deposits of the Niger Delta are divided by the paleo-topographies of underlying relicts of transform fault zones (FZs), such as the Chain, Charcot and Fernando Po FZs (Fig. 1B), into two main lobes: the western Niger Delta lobe (WNDL) and the eastern Niger Delta lobe (ENDL) (Short and Stauble, 1967; Lehner and de Ruiter, 1977; Briggs et al., 2009; Wu et al., 2015). Subsidence rates of up to 200-250 m/Myr and around 350 m/Myr have been estimated for the WNDL (Chima et al., 2021) and the ENDL (Jermannaud et al., 2010; Riboulot et al., 2012), respectively. The two lobes reveal comparable progradation and sediment bypass to the deep oceanic basin during the Pliocene. During the Pleistocene, the WNDL continued to prograde whereas the ENDL mainly retrograded due to still debated factors such as sediment sequestration on the shelf and upper slope linked to the proximity of the Fernando Po transform FZ and to sediment transfer from the ENDL to the WNDL. A subsequent reduction in sedimentary load and deformation rate occurred over the extensional faults of the ENDL (Jermannaud et al., 2010; Rouby et al., 2011; Chima et al., 2020) and translated down-slope to lower rates of shortening in the compressional domain (Jolly et al., 2016).

In the Niger Delta, faults and dipping stratigraphy facilitate the migration of fluids from thermogenic and microbial sources to the base of the GHSZ forming bottom-simulating reflectors (BSRs) (Hovland et al., 1997; Cunningham and Lindholm, 2000; Foschi and Cartwright, 2016) (Fig. 2).

The near-surface gas hydrates and BSR are distributed in two belts that are located in a range of water depths between ~450-1500 m below sea level (mbsl) and ~1200-2800 mbsl, respectively (Hovland et al., 1997; Cunningham and Lindholm, 2000) (Fig. 2). Methane bound in gas hydrates shows a biogenic source prevalence (≥99% of light hydrocarbons, $\delta^{13}C\text{-}CH_4$: –117 to –54 ‰) (Brooks et al., 2000).

A wide range of seafloor fluid seeping structures, such as pockmarks, fluid flow pipes, mud volcanos, gas chimneys and carbonate build-ups commonly occur over folds and major faults

(Haskell et al., 1999; Graue, 2000; Yahaha et al., 2000; Heggland et al., 2001; Kopf, 2002; Løseth et al., 2011; Leduc et al., 2013).

2.2 Study region and previous work

The study region is located on the ENDL and covers a seafloor area of around 80 km by 40 km (Fig. 1B). It is situated in the transitional detachment fold province (Corredor et al., 2005) characterized by little or no deformation interspersed with large detachment folds. The four areas studied herein (pockmark field, mud volcano, area with living benthic macrofauna, and area with slope failures) are located over NW-SE oriented fold/thrust structures resulting mainly from a first compression phase (courtesy of Total SA, Fig. 3):

(i) The pockmark field covers a seafloor area of around 30 km^2 and is located above the northern thrust in water depth ranging from 1100 to 1250 mbsl (Fig. 3). This field is delimited by two major normal faults oriented N130° (Fig. 4A) and lies over the collapsed summit of an anticline (Fig. 4B) (Marsset et al., 2018). It shows a wide range of pockmarks forming either singular pockmarks above faults or pockmark trains above faults and channels (Fig. 4). Different processes such as gas hydrate dissolution, channel dewatering and fluid escape from underlying reservoirs and along fault systems have been proposed to explain their origin (Sultan et al., 2007, 2010, 2011, 2014; de Prunelé et al., 2017; Marsset et al., 2018; Taleb et al., 2018, 2020; Pape et al., 2020). Recurrence of pockmarks within two imbricated sedimentary cycles hypothetically attributed to short-term (around 0.1-0.4 Myr) and long-term (around 1 Myr) stratigraphic sequences described by Jermannaud et al. (2010) suggests a connection with climate/eustatic changes (Marsset et al., 2018).

(ii) The mud volcano is located in the western part of the study region over a thrust in water depth ranging from 1460 to 1625 mbsl (Fig. 3). It was characterized by mudstones near the summit (Bayon et al., 2007; Rongemaille et al., 2011).

(iii) The area with slope failures is located over a thrust front in the eastern part of the study region in water depth ranging from 1650 to 1760 mbsl (Garziglia, 2010) (Fig. 3).

(iv) The area with living benthic macrofauna (formerly called Diapir area; e.g., Bayon et al., 2007; Rongemaille et al., 2011) is confined in a water depth range between 1625 and 1750 mbsl in the southern part of the study region. It is located at the intersection between a fold-and-thrust system and a lateral strike-slip fault attributed to a second compression phase (Fig. 3). Massive carbonate concretions and consolidated shelly sands have been recovered in this area (Bayon et al., 2007; Rongemaille et al., 2011).

The seismic units and sub-units mentioned in the following sections were defined and described in detail in the pockmark field (Fig. 4) by Marsset et al. (2018). These authors identified two seismic units interpreted as turbiditic (UT) and hemipelagic (UH) deposits. These units form a recurrent motif of UT/UH. UT is characterized by channel/levee systems and Mass Transport Deposits (MTDs), that laterally evolve to low-amplitude continuous reflections (Fig. 4B). The youngest UT encompasses the most recent channels located at ~55 meters below seafloor (mbsf) imprinting the seafloor morphology (Figs. 3 and 4). UH shows continuous internal reflections and low-to-moderate acoustic amplitudes (Fig. 4B). The base of the youngest UH is marked by a reflector (labelled R) of regional extent showing flat-shaped high amplitude seismic anomalies (Marsset et al., 2018). Seven sub-units, UH1 to UH7, are identified in the uppermost, youngest unit UH (Fig. 5). The lowermost sub-unit, UH7, is characterized by low-to-moderate amplitude chaotic seismic facies and tends to smooth the topography inherited from channels. UH6 to UH1 are bound at their top by discontinuities related to pockmarks and show low-amplitude parallel reflections. The tops of UH6, UH5 and UH2 are marked by very high-amplitude continuous reflections .

3. Material and methods

Between 2003 and 2011, Ifremer, in partnership with Total SA, investigated the Niger Delta during several cruises including Neris 1 (Voisset, 2003), Neris 2 (Voisset, 2004), ERIG3D (Ker et al., 2010) and Guineco-Mebo (Sultan, 2011) surveys. The results presented here are

based on the analysis of data acquired during these surveys and on data made available courtesy of Total SA.

3.1 Geophysical data and seafloor video documentation

We used a wide range of geophysical data sets (see Table 1 for the synthesis and Supplementary Material A for the detailed description).

Table 1
Summary of geophysical data used and resolutions of devices deployed.

Data source	Geophysical devices			
	Seismic configuration			
	Source	Streamer	Vertical resolution (m)	Frequency (kHz)
Total SA 3D HR Data	2 air-guns	4 multi-channels	5	150
Ifremer Data (Neris1, Neris2, Erig3D)	Near-bottom seismic (SYSIF)	Single channel	0.5/1	0.220-1.05 or 0.650-2.2
	Imagery configuration			
Ifremer Data (Neris1)	Near-bottom side scan sonar (SAR)			170-190

For the whole study region, we used reprocessed 3D high-resolution (HR) seismic data made available courtesy of Total SA. This data set was used mainly to describe the seismic units and plumbing systems, and in particular the fault networks and distribution of fluid-related structures. Seismic attributes such as amplitude and coefficient of correlation were used to provide complementary information on seafloor and sub-seafloor cold seeps.
For a detailed description of each plumbing system, the following tools were used:
(i) 2D very high-resolution (VHR) near-bottom SYSIF (SYstème SIsmique Fond) seismic data acquired by Ifremer (Ker et al., 2010; Marsset et al., 2010). SYSIF data was used to describe sub-units within seismic units, the internal structure of near seafloor fluid-related structures and faults with a resolution higher than the 3D HR seismic. In several profiles, the SYSIF vehicle was equipped with a nephelometer to record water turbidity.

(ii) Near-bottom side-scan sonar SAR (System Acoustique Remorqué) was deployed by Ifremer (https://wwz.ifremer.fr/mediterranee/content/download/38723/file/fiche_sar.pdf) to obtain acoustic backscatter images providing information on seafloor texture and microtopography.

(iii) Near-bottom video system SCAMPI (Système de CAméras Ponctuel Interactif) was deployed by Ifremer (https://www.flotteoceanographique.fr/Nos-moyens/Navires-engins-et-equipements-mobiles/Equipements-mobiles/Camera-embarquee-SCAMPI) to image seafloor features such as living benthic macrofauna and fluid escapes.

3.2 Sediment cores and chronology

A composite sediment core of 53.3 m in -length (spliced GMMB01 and GMMB02 called GMMB01/02 hereafter; internal core codes GeoB16002-1 and GeoB16003-1) was recovered by means of the robotic seafloor drill rig MARUM-MeBo70 (Freudenthal and Wefer, 2013) at a water depth of 1147 mbsl during the Guineco-MeBo survey (2011). The core site (N3°15.1, E6°41.8) is located in the pockmark field NW off the so-called and well-studied pockmark A, in sediments not disturbed at the seafloor by fluid escape structures (Figs. 1, 4 and 5; Sultan et al., 2014; Wei et al., 2015; Pape et al., 2020; Taleb et al., 2020) (see Supplementary Material B).

Lithological characterization of sediment was established from visual descriptions, semi-quantitative X-ray fluorescence spectroscopy (XRF) scanning and grain-size analysis. Characterization of intervals with no core recovery was based on *in situ* P-wave attenuation obtained with the Ifremer PENFELD penetrometer down to 30 mbsf (Taleb et al., 2020). Moreover, the P-wave attenuation curve was considered as a proxy of carbonate (foraminifera)-rich levels (see Supplementary Material B). Chronostratigraphy is based on the comparison of fluctuations of stable oxygen isotopes ($\delta^{18}O$) of planktonic foraminifera with those from Site 1077, ODP Leg 175 (Lower Congo basin; Jahn et al., 2005) whose chronology is based on a correlation with $\delta^{18}O$ signatures of benthic foraminifera from site

677, ODP Leg 111 (Costa Rica rift) (Shackleton et al., 1990). Correlation was also based on a comparison made with the "LR04" stack of benthic $\delta^{18}O$ records compiled by Lisiecki and Raymo (2005). Radiogenic strontium isotope ($^{87}Sr/^{86}Sr$) ratios developed from bulk foraminifera provided additional chronostratigraphic control. The multi-proxy analyses included (see Supplementary Material B for a detailed description):

(i) Semi-quantitative XRF analysis performed with an Avaatech XRF scanner (Richter et al., 2006) at Ifremer, Brest (France). The Ca/Fe ratio was used as a proxy for relative fluctuations of biogenic (Ca) and terrigenous (Fe) sediment sources over time (Croudace et al., 2006; Richter et al., 2006). The Zr/Rb ratio was used as proxy for relative fluctuations of heavy coarse material (Rothwell, 2006) and therefore for lithogenic grain-size fluctuations and as a possible indicator of transport efficiency (e.g., Dypvik and Harris, 2001; Constantinescu et al., 2015).

(ii) Grain-size distribution analysis performed with a Beckman Coulter LS1300 laser granulometer at Ifremer.

(iii) $\delta^{18}O$ analysis of the planktonic foraminifera species *Globigerinoides ruber* performed with a Finnigan MAT251 gas isotope ratio mass spectrometer at MARUM.

(iv) Determination of ratios of radiogenic strontium isotopes ($^{87}Sr/^{86}Sr$) on three foraminifera-rich- bulk sediment samples performed with a Thermo-scientific Triton-thermal ionization mass spectrometer (TIMS) at the Pôle de Spectrometry Océan (PSO) in Plouzané, France.

(v) Compressional wave (Vp) measurements carried out in cores by using an acoustic fork driven into the sediment. One branch of the fork contains a compressional wave source and the second contains the receiver.

(vi) Sedimentation rates were calculated for the various Marine Isotope Stages (MISs; Jahn et al., 2005) identified on sediment core GMMB01/02 from correlation with the multi-proxy analysis (Supplementary material D).

A 0.2-m-long sediment core (N1-KS-07) was recovered from the area with living benthic macrofauna (formerly called Diapir area) ~20 km SW of the pockmark field with a Kullenberg piston corer during the Neris1 expedition (Bayon et al., 2007; Rongemaille et al., 2011).

3.3 Data integration

Seismic profiles and MeBo core GMMB01/02 were integrated into the IHS Kingdom software. MeBo drill core metric length was converted into milliseconds of two-way travel-time (mstwt) using a mean velocity of 1500 m/s (Supplementary Material C, Table C1). The correlation between the seismic and core data provided lithofacies groundtruthing and chronostratigraphic control of seismic sub-units and consequently of the fluid flow structures. This allowed to establish environmental and climate conditions and the timing of waxing and waning of fluid-related structures.

Sediment cores retrieved with the MeBo drill close to pockmark A (see section 3.2) were correlated to the SYSIF profile SYS01-HR-Pr01 in the pockmark field. This provided a general chronologic framework for the fluid-related structures.

4. Results

4.1 Sedimentological facies of deposits hosting fluid seeping structures

Lithofacies have been defined from the composite MeBo sediment core GMMB01/02 recovered in the pockmark field (Fig. 5, Fig. 6A to 6C). They consist primarily of homogeneous bioturbated dark grey mud. The carbonate fraction is dominantly composed of planktonic foraminifera and a few intact or fragmented shells between 50 μm and 1 mm in size (Fig. 6D). It is worth noting that carbonate concretions, which occur repeatedly every 1 to 1.5 m, may have affected correct core recovery and quality (see Supplementary material B). Moreover, a ~10-cm-thick layer of homogenous dolomitic marlstone was recovered at 51.9 mbsf (Fig. 6D).

Based on the biogenic content (foraminifera, shell debris) (Fig. 6D), the P-wave attenuation curve (Fig. 6E), sand content (Fig. 6F) and sediment composition determined by semi-quantitative elemental ratios with the XRF scanner (Fig. 6G and 6H), the multi-proxy analysis resulted in the identification of four characteristic sedimentological facies (Fig. 6I):

Facies 1. *Muddy facies* (Fig. 6I) consists of silty clay with <5 volume % (vol. %) of siliciclastic sand fraction, very low Ca/Fe (0.0-0.2) and low Zr/Rb (0.5-1.5) ratios and a low P-wave attenuation (~20).

Facies 2. *Silty mud facies* (Fig. 6I) consists dominantly of silts with 5-20 vol. % of sand fraction, low Ca/Fe (0.2-0.5) and low Zr/Rb (0.5-1.7) ratios and a low P-wave attenuation (~20-30).

Facies 3. *Sandy mud facies* (Fig. 6I) consists of siliciclastic sand (5-25 vol. %) and silt with a low Ca/Fe (0.0-0.2) and very high Zr/Rb (2.5-4.5) ratios.

Facies 4. *Foraminifera-rich muddy facies* (Fig. 6I) consists of foraminifera-rich siliciclastic mud with high Ca/Fe (0.2-2.0) and high Zr/Rb (1.3-3.0) ratios, and a high P-wave attenuation (30-60). The sand fraction (20-40 vol. %) is related to the abundance of foraminifera.

4.2 Structural features and fault networks

The main structural feature observed on the 3D HR data set for all study sites (Figs. 3, 7A, 8, 9A and 10A) is an antiform affected by a fault network (Figs. 7B, 8B, 9C and 10B). The seafloor fluid-related structures are located at the top of the structural antiform over the fault network. The mud volcano lies above a tight swarm of faults that crosses the top of the antiform up to the overlying volcano root (Figs. 7B and 8B). The area with living benthic macrofauna lies above a dense fault network (vertical offsets of reflectors) that crosses the antiform top and extends into the upper sedimentary hemipelagic layers up to the seafloor (Fig. 9C). A BSR at 300 mstwt (~225 mbsf) (Fig. 9C), marks the base of the GHSZ (see section 2.1). The faults connect down to a probable free-gas bearing reservoir at the base of the GHSZ. This reservoir could be an old channel belonging to a previous UT unit. The

buried channel-levee system named the Bukuma Channel System (BCS) (Zhao et al., 2018) is expressed below the hemipelagic deposits (UH). On SYSIF profiles, numerous stacks of reflector offsets are attributed to crestal faults at the antiform top. A scarp at the antiform top suggests a slight collapse of the crest (Fig. 9D and its zoom). Even though the occurrence of bivalve shells typically hampers penetration of seismic waves in SYSIF data, faults were found to exist underneath areas covered by cemented shells (Fig. 9C). In the area with slope failures, the 3D HR profiles show conjugate faults which outline the collapse of the antiform crest (Fig. 10B). On the SYSIF profiles, the faults exhibit vertical offsets whose amplitudes decrease upward. Most of the faults are capped by upper sedimentary layers 10-20 mbsf (Fig. 11A). The upward decrease in the vertical offsets of faults suggests either 1) an early and abandoned faulting with several episodes of activity, or 2) a unique faulting event in the older formations with vertical displacement decreasing in the upper formation. The only area where faults reach the seafloor is the headwall scarp of a slide (Fig. 11). Several superficial slides marked by hollows of ~10 m high are located on the southwestern flank of the antiform and affect unit UH (SA1, SA2, SA3 on Figs. 10C and 11A; see Marsset et al., 2010 for a detailed description of SA3). The locations of the slides are strongly linked to the fault network. However, unlike other sites, the fault network in this area lacks geophysical evidence of fluid-related structures such as carbonate concretions or associated pockmarks.

4.3 Fluid flow structures

On the 3D HR data, the mud volcano is 4 km in diameter at its base and rises 170 m from the surrounding seafloor. It is located 0.5 km eastward of a channel-levee turbiditic system with associated pockmarks (Figs. 7A and B). The subsurface of the mud volcano displays a characteristic “Christmas-tree” structure ~650 m in vertical extent with at least four (perhaps five) major wedge-shaped packages of extruded mud deposits (i.e., mud flows). The basal part of the mud volcano consists of undifferentiated units interpreted as amalgamated mud extrusions. The mud flows are coeval to regional hemipelagic cover (UH unit, see section 2.2

for the definition of seismic units). The turbiditic units (UT) and particularly the levees of channels commonly onlap the flanks of the preceding mud flow and can overlap its top (Fig. 7B). On SAR imagery, the top of the mud volcano shows superficial small lobes, which are successively and randomly deposited (Fig. 7C and D). These lobes are not draped by hemipelagic deposits and correspond partly to seismic amplitude anomalies (Fig. 7D). This area also hosts small depressions responsible for the late spreading of small lobes (Fig. 7A). During SYSIF deployments in 2004, a high turbiditic event (Fig. 7E) occurred in the water column above the western part of the mud volcano. On the 3D HR seismic, the internal structure of the youngest mud flow (Fig. 7F) consists of at least three stacked and equally developed major lobes (L1 to L3) coeval to UH3 to UH1 (Fig. 8).

In the area with living benthic macrofauna, SCAMPI near-bottom video surveys made across the area (Fig. 9A) revealed dense living benthic macrofauna (bivalves, sea-urchins), suggesting ongoing active fluid flow (Fig. 9E). On the 3D HR seismic bathymetry, this area is characterized by an oblong patch of 1 km by 500 m. This patch is located near the Bukuma Channel System and displays a sinusoidal arrangement of pockmarks (Fig. 9A). The SAR imagery exhibits a large reflectivity anomaly in the patch area (Fig. 9B).

In the area with slope failures, the sediments are not disturbed by fault-related fluid escape structures (see section 4.2). This allowed to obtain good imaging of the stack of UH units (Fig. 10B; Fig. 11) and sub-units UH6 to UH1 (Fig. 11A and its zoom) in the antiform top (Fig. 10A). Turbiditic deposits (UT) and channel-levee systems are preferentially observed in the topographic lows and their pathways are outlined by many pockmarks within UH (Fig. 10B).

5. Interpretation

5.1 Age model and implications for environmental and climate factors

The fluctuations of *Globigerinoides ruber* stable oxygen isotopes (Fig. 6J) show a pattern that can be correlated to regional (Fig. 6K) and global (Fig. 6L) stable oxygen isotope data from MIS 1 until MIS 12 (~420-450 ka) between 34 and 35 mbsf, and possibly until MIS 14 (~550 ka) at ~42 mbsf. The correlation between this age model, the evolution of sedimentological facies (Fig. 6F), and sedimentation rates (Fig. 6M and Supplementary Material D, Table 1) shows that sedimentation fluctuates with glacial-interglacial cycles and suggests a control by northern hemisphere glaciations. Muddy (Facies 1) to silty mud (Facies 2) deposits with high sedimentation rates (10-12 cm/ka) correlate with interglacials MISs (1, 3 5, 7, 9, 11, 13, and possibly 15), which are characterized by warm and humid conditions with enhanced chemical weathering of silicate minerals in the watershed (Zabel et al., 2001). However, during MIS 5 (~65-130 ka), high sedimentation rates of 11-31 cm/ka correlate more specifically with warm and humid substages MISs 5.1, 5.3 and 5.5 (Supplementary Material D). This also suggests a control by the monsoon regime linked to 23 ka precession cycles (Caley et al., 2011). Conversely, foraminifera-rich mud facies (Facies 4) and low sedimentation rates (3-4 cm/ka) coincide with glacial MISs (2, 4 6, 8, 10, 12) and substages MISs 5.2 and 5.4 (Supplementary Material D), which are related to cold and dry periods generally characterized by mechanical erosion of minerals in the watershed (Zabel et al., 2001). During glacial MISs (i.e., MISs 2, 6, 8, and 10), the high Zr/Rb ratios (1.3-3.0) (Fig. 6H) indicate a higher proportion of lithic coarse material possibly linked to a high transport capacity or low clay supply to the ocean. The high foraminifera content is consistent with the findings by Zabel et al. (2001).

Below 35 mbsf, the sediments are mainly composed of muddy facies (Facies 1). A robust chronostratigraphy based on stable oxygen isotope data is not available as these facies are devoid of foraminifera. Between ~45 and 49 mbsf (close to the base of MeBo core GMMB01/02), sedimentological facies fluctuate between muddy facies (Facies 1) to silty mud facies (Facies 2), which may correspond to interglacial periods, and siliciclastic sandy mud

facies (Facies 3), which may correspond to glacial periods. Sandy mud facies are therefore interpreted as turbiditic deposits formed during glacial sea-level lowstands. A low carbonate content below 35 mbsf is likely caused by dilution within terrigenous constituents, as physico-chemical conditions at current water depth of MeBo core GMMB01/02 (1141 mbsl) do not favor carbonate dissolution.

It is worth noting that radiogenic strontium isotopic ratios ($^{87}Sr/^{86}Sr$) indicate ages of 774-797±50 ka (corresponding to MIS 20) at ca. 43 mbsf and of 987±50 ka (corresponding to MIS 26) at ca. 50 mbsf (Fig. 6J). These ages are older than those inferred from $\delta^{18}O$-signatures of *Globigerinoides ruber* (MIS 14 i.e. ~535-562 ka and MIS 18 i.e. ~715-730 ka, respectively, see Supplementary Material D). However, the correlation based on stable oxygen isotopes provides more consistent sedimentation rates for hemipelagic sediments and fine-grained turbidites (Fig. 6M). Indeed, an age of 774-797 ka from $^{87}Sr/^{86}Sr$ instead of 562 ka from $\delta^{18}O$ at 43 mbsf would give a sedimentation rate of ~0.6 cm/ka instead of 5.19 cm/ka for MIS 14 (see Supplementary Material D). We therefore applied these peak-to-peak correlations (Fig. 6M). The results are consistent with our age range for the core. The fact that ages calculated from strontium isotope stratigraphy (SIS) seem to be too old (i.e., $^{87}Sr/^{86}Sr$ too low) can be easily explained by the fact that analyses were conducted on bulk sediment samples. Mixing biogenic carbonates and detrital carbonates that are likely older (i.e., lower $^{87}Sr/^{86}Sr$) can lead to lower $^{87}Sr/^{86}Sr$ in the bulk rock and, therefore, artificially older ages as demonstrated by Pasquier et al. (2019). Moreover, the SIS method lacks precision for time periods <1 Myr as the $^{87}Sr/^{86}Sr$ isotope composition of seawater did not evolve significantly within the last Myr (McArthur et al, 2012).

These results covering the last 700 ka (Pleistocene to Recent) show high sedimentation rates (~8-16 cm/ka) during interglacial periods and low sedimentation rates (~3-4 cm/ka) during glacial periods. We note that the Congo, Nile and Niger deltas show similar patterns with low sedimentation rates during arid periods and high sedimentation rates during arid-humid transitions and humid periods (Ducassou et al., 2009; Picot, 2015; Picot et al., 2019; Laurent et al., 2020).

5.2 Ground-truth calibration of seismic units in the pockmark field

The correlation between seismic and core data at the MeBo drill core GMMB01/02 site (Fig. 6) allows to describe lithostratigraphic and chronostratigraphic characteristics of sub-units UH7 to UH1 (see section 2.2 for the definition of seismic units) from base to top:

- UH7 marks the abandonment of channels and encompasses two intervals of sandy mud facies (Facies 3) indicative of a dominant terrigenous sediment source with turbiditic deposits (Fig. 6F). The top of UH7 is marked by a drastic change to muddy facies (Facies 1), which is interpreted as the end of turbiditic activity. The chronostratigraphy is poorly constrained, but the top of UH7 may correspond to the MIS 16/15 glacial-interglacial transition (~621 ka).
- UH6 to UH2: Each sub-unit is characterized at is base by very low amplitude reflections attributed to muddy facies (Facies 1) evolving upward to silty mud facies (Facies 2), and at its top by high-amplitude parallel reflections attributed to foraminifera-rich mud facies (Facies 4). Tops of sub-units UH6, UH5, UH4, UH3 and UH2 (UH1?) are correlated with MIS 14/13, MIS 12/11, MIS 10/9, MIS 8/7, MIS 6/5 (MIS 2/1?) glacial-interglacial transitions.

The 100 ka duration of each sub-unit UH6 to UH1 is in agreement with the development of prograding wedges on the continental shelf in response to glacial-interglacial fluctuations (Riboulot et al., 2012). This is also consistent with the short-duration (around 0.1-0.4 Myr) stratigraphic sequences previously identified by Jermannaud et al. (2010). Based on the chronology of a nearby reference core not affected by any fluid seepage (see the 10.6 m long N1-KSF-39 core in Bayon et al., 2015), Marsset et al. (2018) estimated a mean hemipelagic sedimentation rate around~8 cm/ka. This estimate implied an age of ~1 Ma for the base of the youngest UT unit and thus a duration of ~1 Myr for the UT/UH cycles. This is consistent with the age of at least 700 ka based on the $\delta^{18}O$-signatures of *Globigerinoides ruber* (Fig. 6J) for sub-unit UH7, which corresponds to the base of the youngest, uppermost unit UH. This is also consistent with the 1 Myr sequences described by Jermannaud et al. (2010). The correlation between the UT/UH cycles and UH6 to UH1 sub-units with these

long- and short-duration sequences confirms the hypothesis of Marsset et al. (2018). Comparable durations of ~1 Myr have been calculated for such UT/UH cycles in the WNDL (Chima et al., 2020). The very high amplitude R regional reflector located at the base of the youngest UH on HR seismic is attributed to the Maximum Flooding Surface 'MFS1' (Rouby et al., 2011) of the long-term (~1 Myr) stratigraphic sequence described by Jermannaud et al. (2010). The MFS is the inversion from retrogradation (below) to progradation (above). Within marine sections, the MFS is often a lithologically condensed section rich in microfossils (e.g., Gutierrez Parades et al., 2017). MFS1 was estimated to have been deposited at ~600 ka (Rouby et al., 2011).

5.3 Ground-truth calibration of pockmarks in the pockmark field

Correlation of the seismic data with core data at the MeBo drill core GMMB01/02 site shows that buried pockmarks at the tops of sub-units UH6 to UH4 have formed in foraminifera-rich muddy facies (Facies 4) during glacial periods, with low sea level and low sedimentation rate conditions (Fig. 6). Pockmarks were not identified in UH7 sandy mud facies (Facies 3), although conditions were favorable for fluid migration and seafloor discharge (e.g., glacial periods, low sea level and low sedimentation rate; see section 5.1). The pockmarks are sealed by deposits belonging to muddy facies (Facies 1) to silty mud facies (Facies 2). These deposits formed during interglacial periods, when high sea level and high sedimentation rates prevailed. In a previous study, two types of pockmark developed by two main distinct processes were identified within UH (Marsset et al., 2018): Type 1 (from UH6 to UH4) resulting from no or low sediment deposition attributed to fluid escape associated with seafloor settlement (benthic macrofauna, carbonate precipitation, gas-hydrate formation) and Type 2 (from UH3 to UH1) resulting from post-depositional erosion, caused by collapse (possibly due to gas-hydrate destabilization through dissolution) (Fig. 5). The transition from Type 1 to Type 2 pockmarks was explained by a decrease in fluid flow during the formation of UH. The multi-proxy analysis performed in this study (Fig. 6) shows that the Type 1-Type 2

transition occurred during MIS 8 lowstand marked by high carbonate content (Fig. 6G) and low sedimentation rates (Fig. 6M) indicative of low terrigenous supply.

5.4 Definition and comparison of plumbing systems

A synthesis on the cold seep of the study region highlights the role of compressive tectonics linked to gravity-driven deformation on the distribution and architecture of plumbing systems (Fig. 12). Dense patterns of extensional faults, which likely serve as conduits for upward fluid migration, have formed in the antiform crests during or after compressive phases. The diverse fault networks characterizing the plumbing systems suggest strong spatial variability in the leakage mechanisms that promote fluid migration. It is worth noting that in the area with slope failures, a fault network without associated fluid-related structures suggests that processes other than deformation control the presence of fluid-related structures. These processes are environmental variations of source rock deposition and their evolution in terms of burial, maturation, migration and trapping history (Stacher, 1995; Katz, 2003). The diverse fluid flow structures in the study region indicate a strong variability in fluid seeping (Fig. 12). The “Christmas-tree” structure of the mud volcano reflects episodic eruptions (see e.g., Kopf, 2002 for an explanation; Yusifov and Rabinowitz, 2004; Stewart and Davies, 2006). The results highlight successive cycles of mud extrusion during UH and quiescence during UT. The complete covering of mud flows, including the conduit feeding the mud flow, by the distal parts of UT channel levees is evidence of a halt in mud flow activity and/or a rapid accumulation of turbiditic deposits preventing mud extrusion. Newly developed conduits that breached the levee deposits and facilitated vertical fluid flow are evidence of mud flow activity resuming and/or a halt in turbiditic deposits. A progressive decrease in the diameter of the youngest lobe L3, displayed by the reduced extent of superficial small lobes at its top, favored the progressive hemipelagic draping of the external parts of the mud volcano (Fig. 7D; Fig. 8A). This reveals that the mud volcano is currently less active than in the past.

However, high turbidity recorded close to the top of the volcano suggests ongoing mud volcanic activity.

The present-day low activity of the mud volcano is coeval to the destabilization of pockmarks located at the seabed and attributed to a local decrease in gas flow from the base of the gas-hydrate occurrence zone (Sultan et al., 2010, 2014). Hydrate dissolution releasing water and gas has been invoked to explain the destabilization of pockmarks (Sultan et al., 2010, 2014). The coeval recurrence of mud flows and pockmarks is controlled by the sedimentary cycles UT/UH correlated to long- (~1 Myr) and short-duration (0.1 Myr) stratigraphic sequences (Fig. 12). These sequences are attributed to forcing factors such as climate, eustasy, subsidence and sedimentary supply (Jermannaud et al., 2010; Riboulot et al., 2012). The impact of these forcing factors on sedimentation rates, and on sediment distribution and deformation, as well as their implications for fluid flow structures are discussed for short- and long-duration time scales.

6. Discussion

6.1 Fluid flow controlling factors over glacial-interglacial time scales

6.1.1 Conditions not conducive to seafloor fluid expulsion during interglacial periods

Our results show that high sedimentation rates (~11 cm/ka) of fine-grained muddy sediments deposited during interglacial highstands were not favorable to fluid expulsions (Fig. 13A). The high sedimentation rate of ~16 cm/ka calculated for MIS 1 i.e., 11 ka to present (Supplementary Material D, Table 1) corroborates the high values of sedimentation rate on the continental slope after 12 ka which are coeval to the highest river discharge rates (Pastouret et al., 1978; Pokras, 1987; Lezine and Cazet, 2005; Bayon et al., 2015). Fluvial input gradually increased from 15.5 cal ka BP and reached a maximum between 12.4 and

8.2 cal ka BP in relation to increased precipitation caused by intensification of West African monsoons (Maley and Brennac, 1998; De Menocal et al., 2000; Cole et al., 2009). The increase in river discharge has controlled the deposition of fine-grained terrigenous material (Pastouret et al., 1978). Moreover, during this period of relatively fast sea-level rise, terrigenous material was eroded in relatively high portions from the continental shelf and re-deposited towards the Niger fan (Kallweit et al., 2012). As for MIS 1, MIS 5 i.e., ~65-130 ka and more specifically humid periods MISs 5.1, 5.3, and 5.5 are characterized by a high sedimentation rate (Fig. 6M). A significant river discharge is reported for MIS 5.1 from a core located off the coast from the Sanaga river mouth in west Cameroon (Weldeab et al., 2007). A possible concurrent high fluvial input of the Niger river may explain the high sedimentation rate recorded in GMMB01/02 (31 cm/ka, Fig. 6M) and on the upper slope (Riboulot et al., 2012).

During highstands, the Niger deltaic region was located far from the shelf edge and both the Niger fluvial input of fine-grained suspended terrigenous material and eroded sediments from the shelf flowed towards the slope and the basin. Consequently, the low sedimentary load on the shelf is considered to have been insufficient to generate gravity-driven deformation and subsequent fluid expulsion (Fig. 13A). Likewise, the high sea level increased the hydrostatic pressure in the sediments of the continental slope preventing fluid expulsion.

6.1.2 Conditions conducive to seafloor fluid expulsion during glacial periods

Our results show that low sedimentation rates (~4 cm/ka) of hemipelagic sediments deposited during glacial lowstands were favorable to fluid expulsion. The hemipelagic layers are relatively coarse-grained (foraminifera-rich) (see Section 4.1) and porous and have favored fluid migration as evidenced by the presence of gas hydrates in such layers within pockmarks (Taleb et al., 2020; Supplementay Material B). Low sedimentation rates have favored seafloor fluid expulsion and formation of cold seeps (see section 1). From 40 to 15.5 cal ka BP, i.e., during the last glacial and arid period, only scattered river discharges

occurred (Lezine and Cazet, 2005; Lézine et al., 2005), which may explain the low sedimentation rates during this period. Previous studies in the WNDL show that glacial periods, at least over the last 150 ka, were characterized by the occurrence of channel-levees linked to tributaries of the Niger River (Jobe et al., 2015). These channels were active only during lowstands (e.g., MIS 6, ~130 ka) and during sea-level falls (e.g. at ~50 ka during MIS 3) when the canyons were connected to the rivers (Allen, 1964; Burke, 1972; Olabode and Adekoya, 2008; Jobe et al. 2015). However, channels associated with glacial periods were not found in our data sets. As mentioned above (see section 1), a low sea level provokes a decrease in hydrostatic pore pressure in fluid reservoirs resulting in gas exsolution. Two types of reservoir can be considered in this study: i) Shallow fluid reservoir: a decreasing sea level leads to an upward migration of the base of the GHSZ, a decay of gas hydrates below, and consequently gas release (e.g., Foucher et al., 2002). However, further studies considering parameters such as regional bathymetry and precise position of the BSR relative to the coastline will clarify the hydrate-related processes occurring during sea-level falls; ii) Deeply buried reservoir: these reservoirs are located below unpermeable sediments responsible for the accumulation of overpressurized fluid, which is a widespread process within the Niger Delta (Mourgues et al., 2009 and references herein). The drop in hydrostatic pressure during the Last Glacial Maximum lowstand has already been invoked to explain pockmark formation on continental margins (Lafuerza et al., 2009, Davy et al., 2010; Plaza-Faverola et al., 2011) and on the ENDL continental shelf and slope (Riboulot et al., 2013). It may also explain the formation of the pockmark field in the northern part of the study region. However, a deep thermogenic source was also identified for the formation of pockmarks in the study region (Ruffine et al., 2013; de Prunelé et al., 2017) suggesting an origin in the mobile shales of the Akata formation. This mobilization of shales is invoked for the deep source fluid migration to the pockmark field and the mud volcano in the study region. The mobility of shales and the pervasive deformation and faulting in Pleistocene to Recent deposits of the Niger Delta is driven by sediment load. We postulate that the development and loading of prograding wedges on the continental shelf during sea-level drops induced

gravity-driven deformation leading to syn-depositional deformation in the hanging walls of growth faults (Corredor et al., 2005; Rouby et al., 2011; Riboulot et al., 2012) and to the migration of fluids to the pockmark and mud volcano areas. The conjunction of high deformation and high sedimentation rates of relatively permeable sediments is already invoked in the development of overpressure and mud volcanism (Pinheiro et al., 2006; Bonini, 2008; 2012; Medialdea et al., 2008; Deville et al., 2010).

6.2 Controlling factors of sedimentation and deformation over long-term (1 Myr) time scales

6.2.1 Conditions not conducive to seafloor fluid expulsion during the turbiditic phase

The absence of pockmarks in UT layers revealed that turbiditic activity did not favor seafloor fluid expulsion. The presence of channel-levee systems within UT may prevent fluid expulsion as channelized systems are known to be characterized by very high sediment accumulation rates (Mikkelsen et al., 1997; Lombo Tombo et al., 2015). Periods of channel filling were also unfavorable for fluid expulsion as pockmarks are not found in seismic sub-unit UH7 (Fig. 6C). The persistent supply of fine turbidites at high sedimentation rates (~9 cm/ka) during sea-level lowstands of UH7 (possibly MIS 18 and MIS 16) may explain the absence of pockmarks (Fig. 6L and 6M).

The chronostratigraphy from core GMMB01/02 illustrated that channels visible on the seafloor and located at ~50-60 mbsf (Fig. 4) formed at ~1 Ma and that the end of the turbiditic activity (UH7 top) corresponds to the MIS 16/15 glacial-interglacial transition (621 ka) (see section 4.2). These channels belong to the youngest turbiditic unit UT of the long-term sequence UT/UH of the study region (Fig. 6B) and more widely of the Niger Delta (Jermannaud et al., 2010; Zhao et al., 2018; Chima et al., 2020). They may have been connected to the Niger River in the 1.3-0.6 Ma interval when both sedimentary progradation and deformation strongly increased in the western part of the ENDL (Rouby et al., 2011). This period of turbiditic activity also corresponds to the Middle Pleistocene Transition (~0.8-

1.0 Ma) which is marked by the increasing amplitude of glacial-interglacial sea-level variations (Lisiecki and Raymo, 2005), and fluctuations in low-latitude (semi-) precessional insolation (De Menocal, 1995; Dupont et al., 2001).

6.2.2 Conditions conducive to seafloor fluid expulsion during the hemipelagic phase

Gravity-driven deformation was limited in the ENDL since MIS 16/15 and is coeval to a limited progradation of the delta front (Rouby et al., 2011). However, we consider that deformation since MIS 15 was still sufficient to facilitate fluid expulsion in the prevailing hemipelagic sedimentation since MIS 16/15. According to Riboulot et al. (2012), the MIS 12 to MIS 8 interval was characterized by a general progradation/aggradation pattern in the eastern part of the ENDL, which was caused by sediment supply rates outpacing accommodation rates. During MIS 8, an apparent major retrograding trend marked by backstepping deposits, was attributed to subsidence outpacing sediment accumulation (Riboulot et al., 2012). The location of backstepped deposits far from the shelf edge likely led to subsequent reduction in the sedimentary load and deformation rates on the present-day extensional province and, therefore, to lower gravity-driven deformation rates in the transitional and compressive domains of the Niger Delta. This may explain the morphological change of pockmarks from Type 1 to Type 2, which is interpreted as a decrease in upward fluid flow (see section 5.3 and Fig. 6C). Similar or even exacerbated conditions during MIS 4 may explain the absence of pockmarks.

7. Conclusions

This study on the Nigerian continental slope shows that seabed fluid-related structures such as a pockmark field, a mud volcano and an area with living benthic macrofauna typical of active fluid flow, are fueled by a range of plumbing systems with diverse fault networks.

Even if all seabed fluid seeping structures are associated with underlying thrust-and-fold structures, the contrary is not necessarily verifiable. The highly deformed zone (outer fold and thrust belt) seems conducive to the development of the mud volcano and the area with living benthic macrofauna, while the pockmark field developed far from the highly deformed zone. Pockmarks formed during glacial sea-level lowstands when conditions were favorable for fluid expulsion including low sea levels, formation of coarse-grained (foraminifera-rich) muddy deposits, and low sedimentation rates. Conversely, conditions during interglacial sea-level highstand periods were unfavorable for fluid expulsion and inhibited pockmark formation. These conditions correspond to periods of high sea level and high sedimentation rates of muddy deposits. Over long-term timescales (~1 Ma), pockmarks and major wedge-shaped packages of extruded mud deposits occur recurrently during the hemipelagic phase and not during the turbiditic phase.

As with other monsoon-influenced African fluvial systems such as the Congo and Nile rivers, it is probable that during glacial and interglacial periods river-driven sediment supply controlled by monsoon-driven climate changes were the main factors influencing the sediment transfer and distribution along the Nigerian margin. We postulate that during lowstands, sea-level drops, sediment progradation on the shelf and gravity-driven sediment deformation, which were enhanced, have caused pockmark formation and mud extrusion on the continental slope.

We hypothesize that cyclic gravity-driven sediment deformations controlled by glacial-interglacial and long-term variations in accommodation and sedimentation affect the cyclic evolution of plumbing systems and the type of pockmark since the Plio-Pleistocene. In this study, we demonstrate that the continental margin of the Niger Delta is a dynamic system where sedimentary and tectonic processes on the continental shelf have an impact on fluid flow on the continental slope on short-term (around 0.1-0.4 Ma) and long-term (1 Ma) timescales since the Plio-Pleistocene.

Declaration of competing interest

Co-authors agree with all the content presented in this contribution, and claim no conflict of interest.

Acknowledgements

This work was supported by projects Neris, ERIG3D (collaboration between Total SA, E. Cauquil and D.H. Drapeau and Ifremer, M. Voisset) and Guineco-MeBo (collaboration between Ifremer and MARUM). Ifremer data were acquired during surveys Neris 1, Neris 2 and ERIG3D. N. Sultan, B. Marsset, S. Ker, P. Vagner, V. Chevalier, S. Calassou, E. Thereau, S. Garziglia and the PAS laboratory (GM-LGS) are greatly thanked for their scientific and technical contribution. Thanks to H. Kuhnert (MARUM) for $\delta^{18}O$ measurements on foraminifera. We also thank Total SA (D.H. Drapeau, E. Cauquil), who provided reprocessed exploration 3D HR seismic and AUV datasets and structural interpretation. Thanks are extended to the scientific staff and crew of Ifremer, GENAVIR, and MARUM who operated the ships (R/V Le Suroît, R/V L'Atalante, R/V le Pourquoi Pas?) and equipment during expeditions at sea (Neris1; Neris2; ERIG3D and Guineco-MeBo (2011)). The manuscript greatly benefited from critical reviews from Dr A. Portnov (University of Texas, Austin) and two anonymous reviewers on a previous submitted version. We also thank Eric Deville (Ifp-EN, Rueil-Malmaison) for fruitful discussions and A. Chalm for proof reading the text.

Figures

Fig. 1. Tectono-sedimentary context of the Niger Delta. A) Location of the Niger Delta and progradation of the delta over the Cenozoic; LME: Lower Middle Eocene; UME: Upper Middle Eocene; UUE: Upper Upper Eocene; Oli: Oligocene; O/M: Oligo-Miocene; Mio: Miocene; UM/P: Upper Miocene-Pliocene; P/P: Plio-Pleistocene (from Short and Stauble, 1967). B) Structural map of the Niger Delta and locations of the study region (red box), the composite MeBo drill core GMMB01/02 (sample identifiers GeoB16002-1 and 16003-1, this study), and the regional dip section presented in Fig. 13. The western and eastern Niger Delta lobes (WNDL, ENDL) and the Chain, Charcot and Fernando Po Fracture Zones (FZs)

are indicated. C) Synthetic cross-section of the Niger Delta showing the main structural domains (extensional, transitional and compressional from NNE to SSW) and the prograding depocenters. B and C are extracted from Rouby et al. (2011). D) Synthetic cross-section through the Niger Delta showing the three sedimentary formations (Benin, Agbada and Akata) (from Jermannaud et al., 2010, modified after Saugy and Eyer, 2003). E) Major structural provinces and location of the study region (red box) (modified from Corredor et al., 2005).

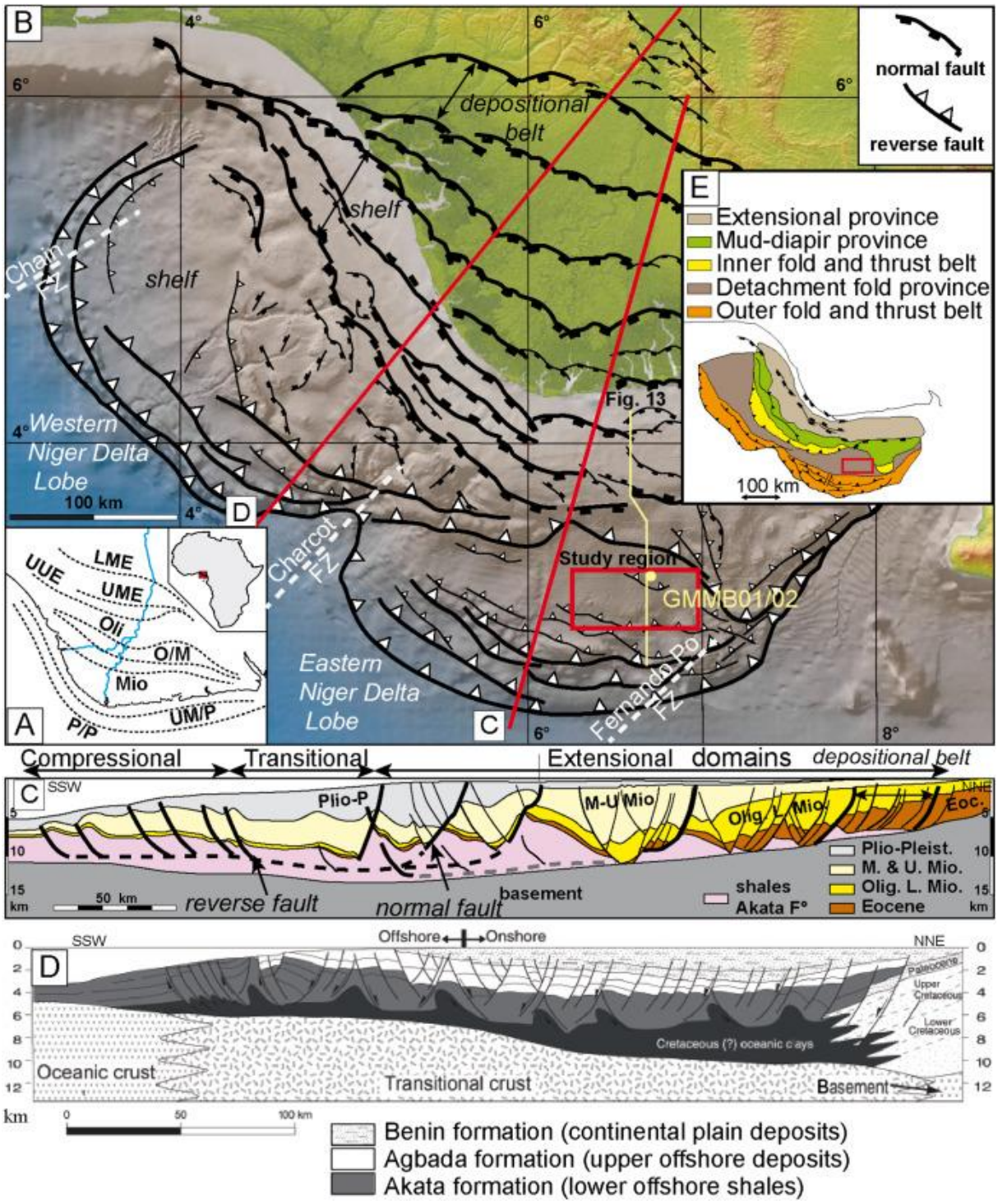

Fig. 2. Geographical location of gas hydrates collected from near-surface sediments (red triangles) on the Nigerian continental margin. Bottom-simulating reflectors (BSRs) mapped by Cunningham and Lindholm (2000) are shown in dark blue. Open circles correspond to core locations (from Brooks et al., 2000). The study region is indicated by the red box.

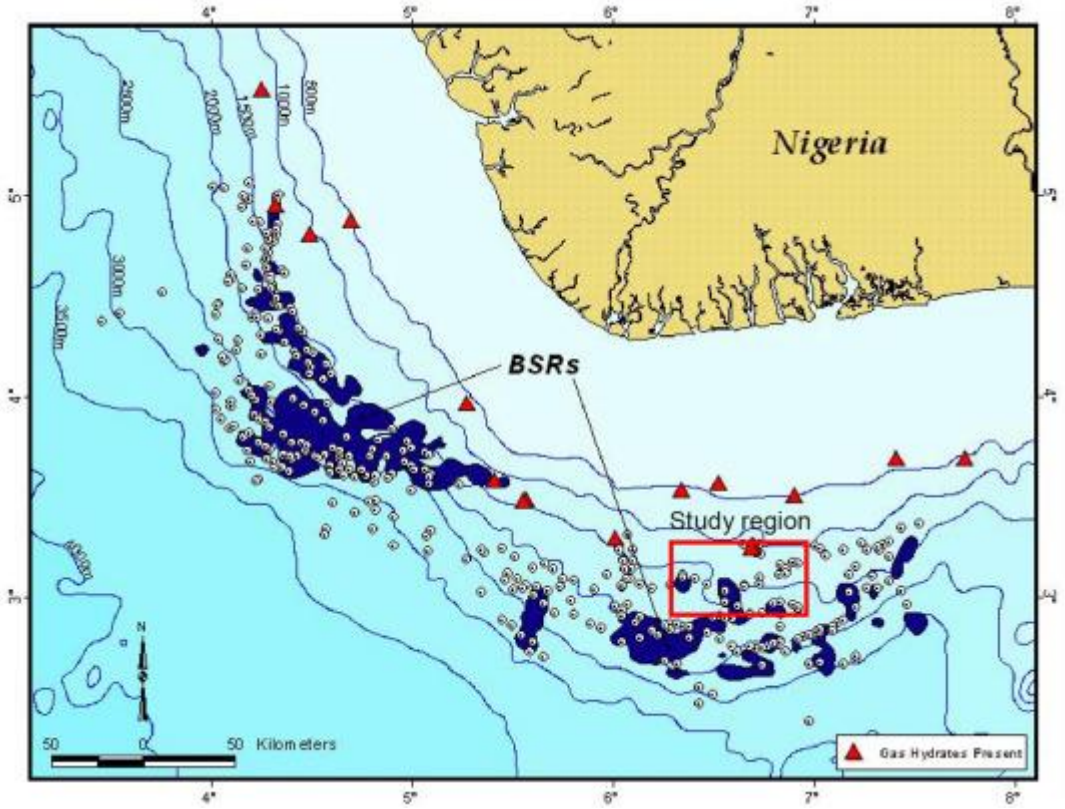

Fig. 3. 3D HR seismic bathymetry with superposed structural map indicating the distribution of NW-SE trending fold/thrust structures, the left lateral strike-slip fault and the bi-axial compression (courtesy of Total SA). The four areas investigated in the study region (see Fig. 1B for its location) are indicated by black boxes.

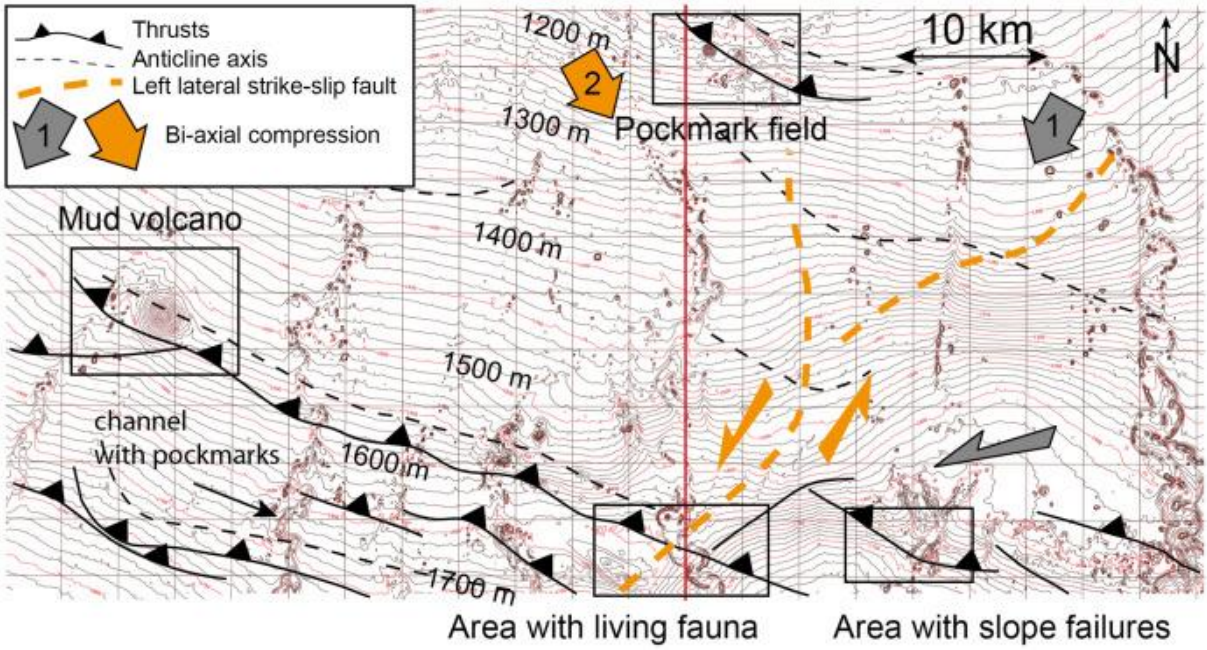

Fig. 4. Geomorphology of the pockmark field (modified from Marsset et al., 2018). A) Bathymetric map based on Autonomous Underwater Vehicle (AUV) data (George and Cauquil, 2007), with locations of SYSIF (SYstème SIsmique Fond) profile SYS01-HR-Pr01, the 3D HR seismic line (see Fig. 4B), as well as MeBo drill core site GMMB01/02 (yellow point NW of pockmark A). Note the distribution of fluid flow structures within a NW-SE trending graben bounded by two structural northern (NL) and southern (SL) lineaments, i.e., major faults. The recent N-S trending buried channels recognized below the seabed and major faults are projected on the map (extracted from Sultan et al., 2014). B) 3D HR seismic line (see location on Fig. 4A) showing the graben with faults and bounded by NL and SL at the top of the antiform. Note the main types of seismic units (UH, interpreted hemipelagic phase, and UT, interpreted turbiditic phase with MTDs locally) (from Marsset et al., 2018).

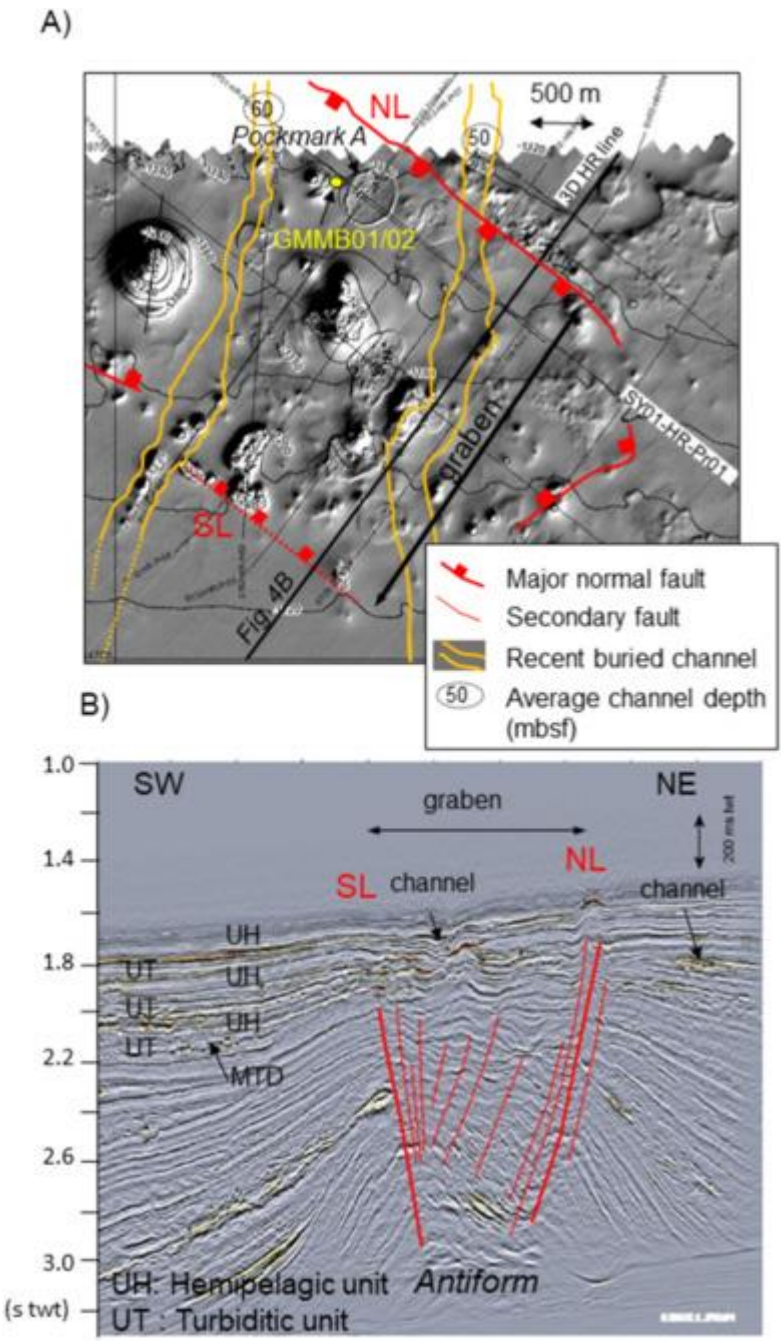

Fig. 5. Location of MeBo drill core GMMB01/02 projected on seismic profiles. A) The SYSIF profile SYS01-HR-Pr01 (for location see Fig. 4A) and superimposed interpretative line drawing (modified from Marsset et al., 2018) show the MeBo drill core close to pockmark A and across the youngest UH unit comprising sub-units UH1 to UH7. Note the buried pockmark X and the poor morphological expression of the channel within UT. B) Zoom on raw seismic data showing position and length of the MeBo drill core and cored sub-units UH1 to UH7. C) Line drawing of pockmark A located at the seabed and interpreted as an erosional depression (Type 2). Note the two erosional sidewalls of the pockmark giving a ring-shaped depression at the seabed (Fig. 4A), and the patch-shaped seismic anomaly in orange color. D) Line drawing showing pockmarks stacked from sub-units UH6 to UH4 interpreted as non-depositional depressions (Type 1). Note the flat-shaped seismic anomalies in orange color. Note also the depositional hiatus in the center of pockmark X located at UH4 top and deposit thinning at its sidewalls (see Marsset et al., 2018 for details).

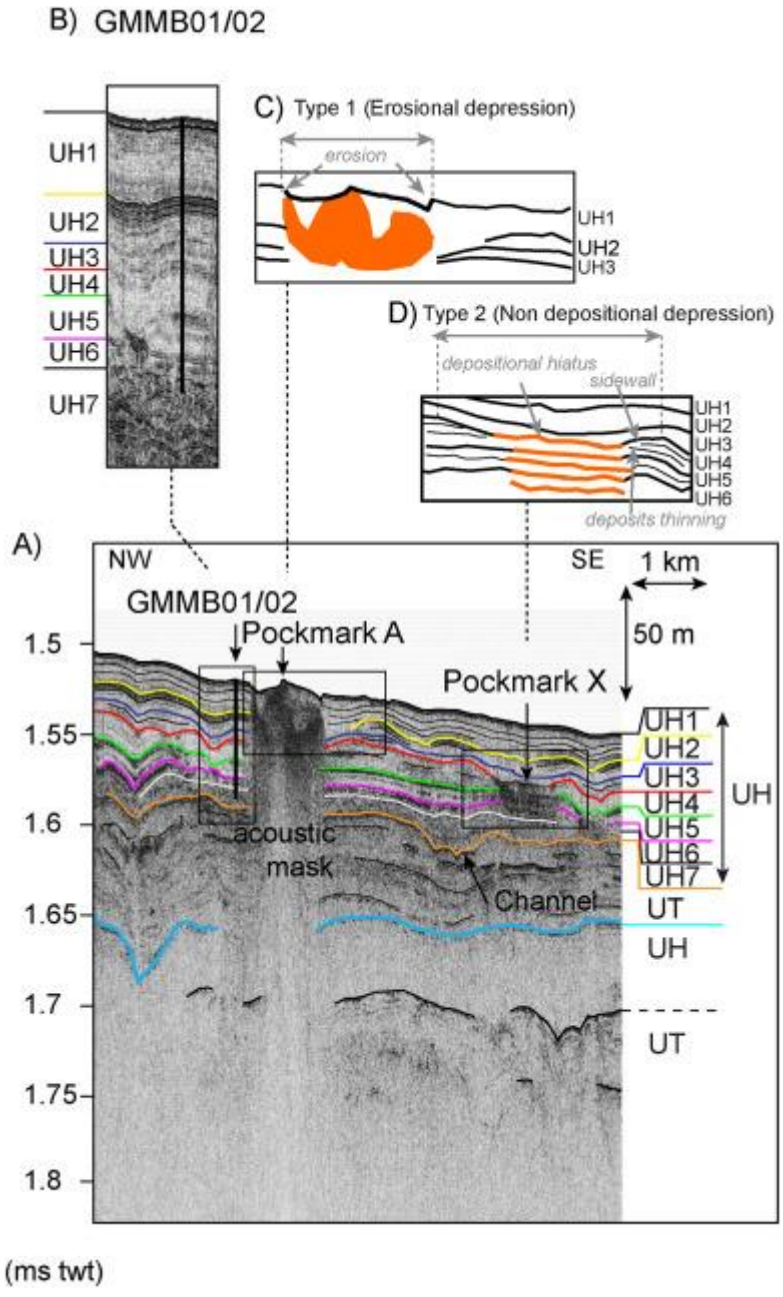

Fig. 6. Calibration of seismic units and pockmarks (pockmark field) by multi-proxy analysis at the MeBo drill core GMMB01/02 site. A) Sysif profile SYS01-HR-Pr01 at the GMMB01/02 site. B) Log of seismic units at site GMMB01/02. C) Synthetic log of pockmark distributions distant to site GMMB01/02 (see caption below based on the interpretation of Marsset et al., 2018). D) Lithologic log of core GMMB01/02 with indication of gaps in recovery and biostratigraphy (see caption below). E) Penfeld P-wave attenuation curve (GMPFV-07-S1 at site GMMB01/02). F) Grain-size percentages following five classes (see caption below) and superimposed sand (i.e., >63 μm) percentages (blue curve). G) Ca/Fe ratio from XRF scanner. H) Zr/Rb ratio from XRFscanner. I) Sedimentological facies (see caption below). J) $\delta^{18}O$ curve of planktonic foraminifera with superimposed $^{87}Sr/^{86}Sr$ dating on bulk foraminifera (red values). K) $\delta^{18}O$ curve from site1077, ODP 175 (Jahn et al., 2005). L) $\delta^{18}O$ curve from the composite global "LR04" $\delta^{18}O$ stack (Lisiecki and Raymo, 2005). M) Sedimentation rates calculated for sediment core GMMB01/02. Light blue horizontal areas highlight the proposed correlations.

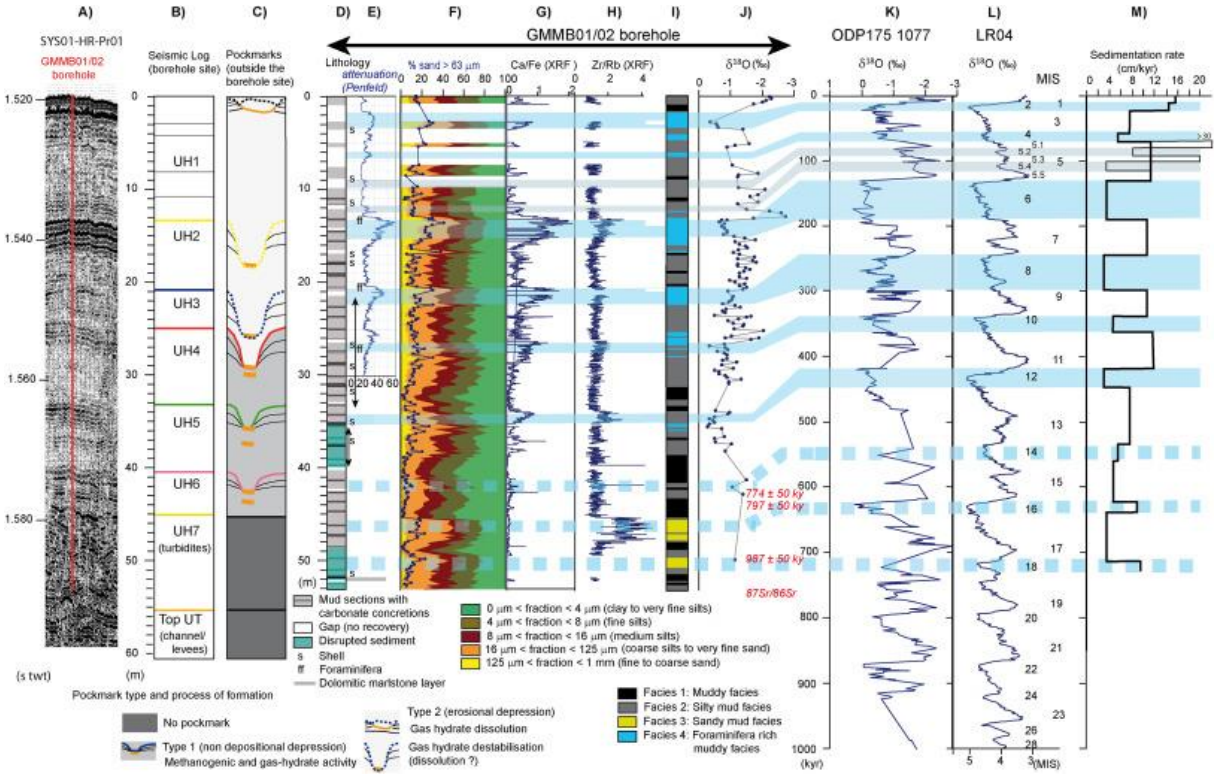

Fig. 7. Geomorphology of the ‘Mud volcano’ area. A) 3D HR seismic bathymetry showing the location of the mud volcano with mud outlets forming seafloor depressions, a channel-levee system with pockmarks, as well as orientations of seismic profiles (black solid lines) and SAR (Système Acoustique Remorqué) grid (blue dotted lines). B) 3D HR line on SAR profile N1SAR54 showing the mud volcano located above a tight swarm of faults. Stacked mud flows have formed a “Christmas tree” structure. Note the UT/UH motif, the levee, which overlaps an old mud flow and exhibits a fracture above the faults and the interpreted turbidites ponded in the basins located on either side of the antiform. C) SAR profile N1SAR54 showing superficial lobes on the mud volcano top. D) 3D HR amplitude seismic attribute with superimposed superficial lobes identified from SAR imagery. Low amplitudes (orange) correspond to hemipelagic deposits while high amplitudes (blue) correspond to lobate mud flow deposits. E) Top: Nephelometric measurements revealing enrichment of suspended material in the water column around 100 meters above the seafloor (values >2 Nephelometric Turbidity Unit (NTU)). Bottom: SYSIF profile N2CH37 recorded in 2004 (cruise Neris 2) showing the youngest mud flow (green dotted line drawn from subfigure F). F) 3D HR seismic line 6 close to N2CH37.

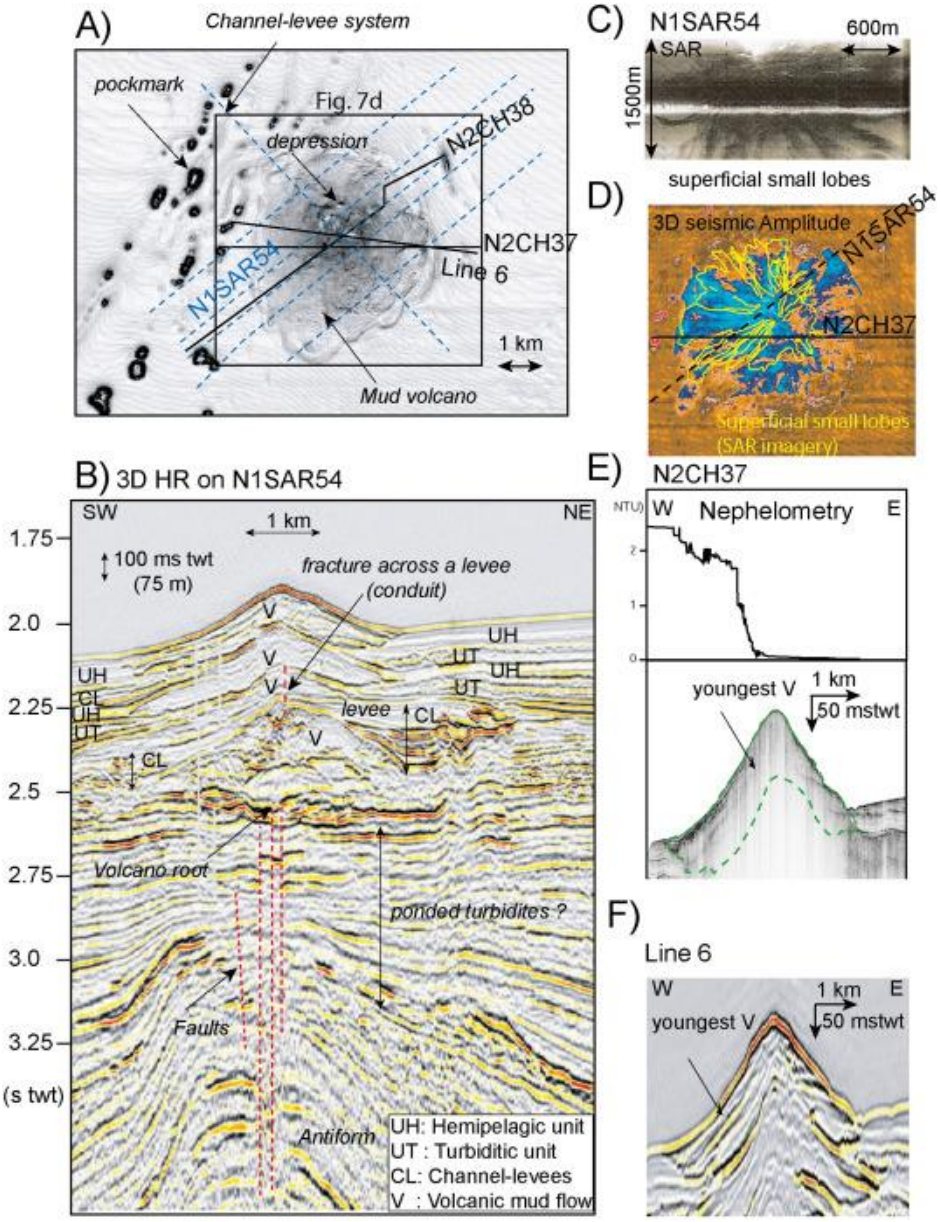

Fig. 8. Internal structure of the youngest mud flow at the mud volcano. A) SYSIF profile N2CH38 showing intercalations between the three lobes (L1 to L3) forming the youngest volcanic mud flow and seismic sub-units UH4 to UH1. Note the UT (distal part of a levee) and overlying sub-units UH7 to UH5 which onlap the previous mud flow. B) 3D HR line 6 showing the three lobes L1 to L3. Note the faults in the deeper structure of the volcano. C) Map showing the location of the lobes identified with the 3D seismic correlation coefficient attribute, and the location of small superficial lobes identified with side scan sonar (SAR).

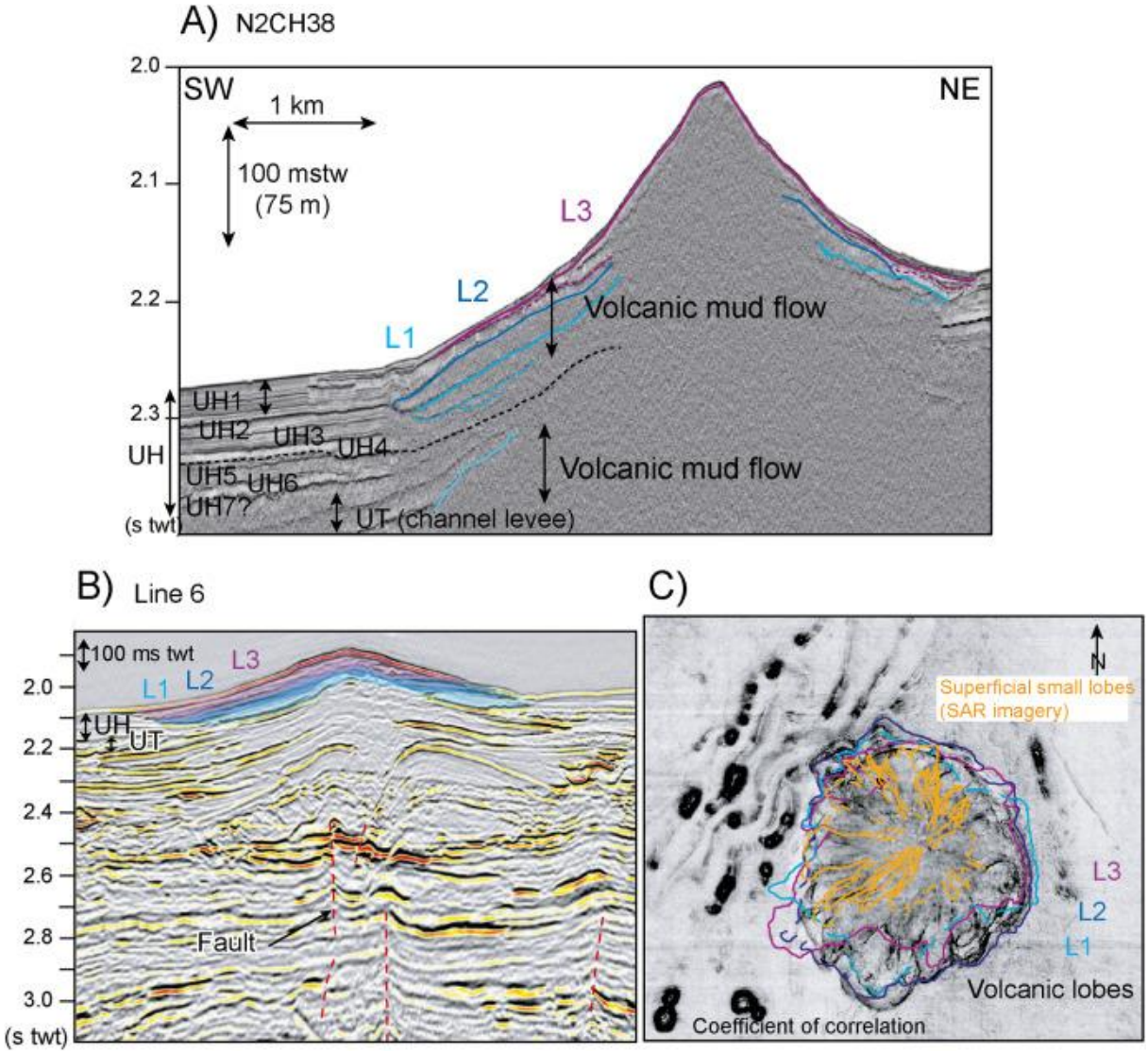

Fig. 9. Geomorphology of the area with living benthic macrofauna. A) 3D HR seismic bathymetry with locations of seismic profile N2CH34, SAR profile N1SAR69, and sediment core N1-KS-07 (see Bayon et al. (2007) and Rongemaille et al. (2011) for sediment composition). Note the location of the high reflectivity patch ('patch') and the Bukuma Channel System (BCS) with pockmarks. B) N1SAR69 profile (imagery) showing the acoustic facies of the patch. C) 3D HR line located on N2CH34 showing the location of the area at the top of the antiform and the fault network. Note the channel-levee system draped by deposits assigned to the hemipelagic unit (UH) and the presence of the BSR. D) SYSIF profile N2CH34 showing the fault network reaching the seafloor (see the zoom) and the location of core N1-KS-07, that retrieved consolidated sediments generating the acoustic mask underneath. E) Scampi video sledge record of the seafloor showing dense living benthic macrofauna at the top of the antiform at the scarp (see location of the scarp in D).

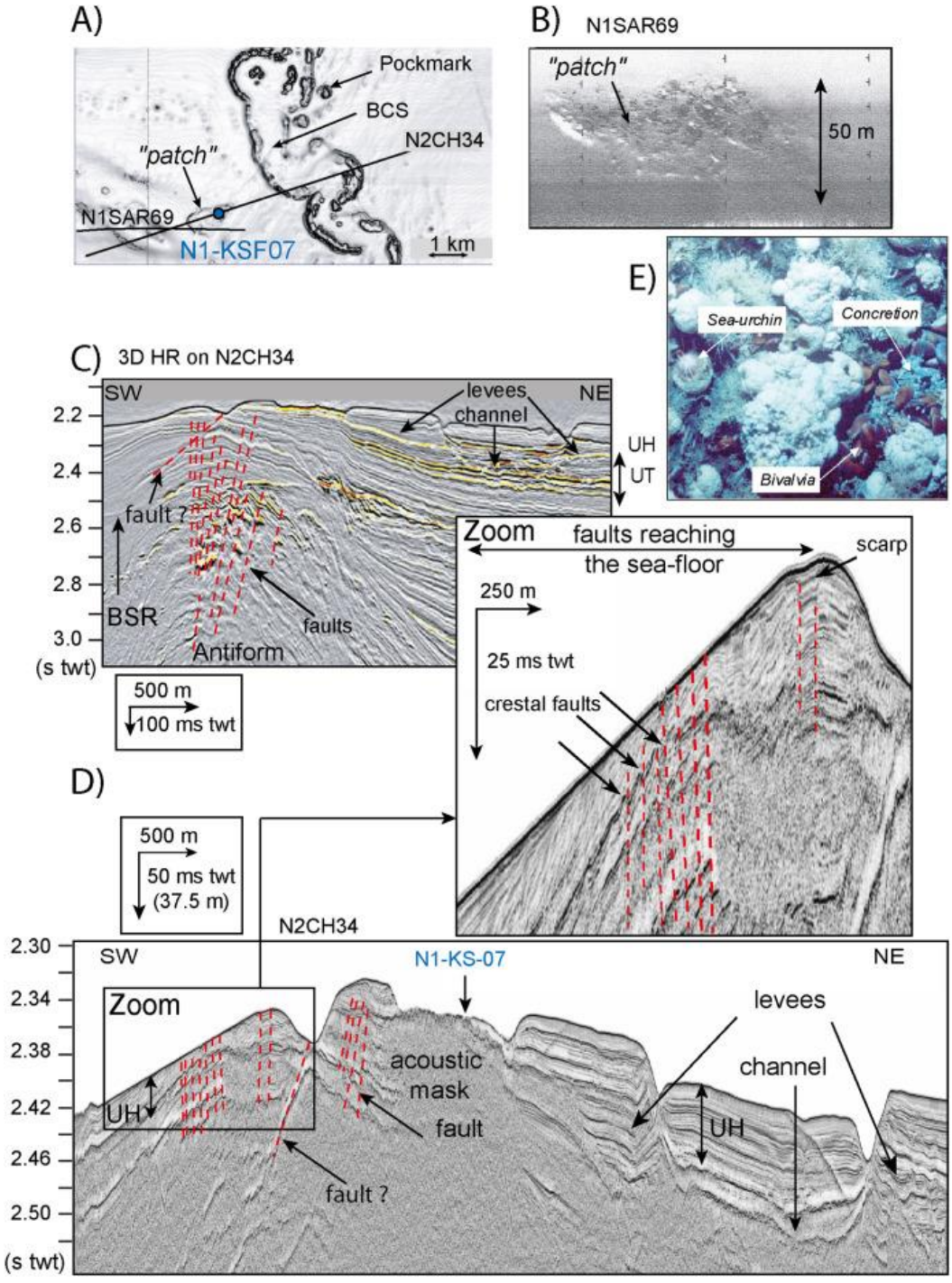

Fig. 10. Area with slope failures. A) 3D HR seismic bathymetry with location of the area with slope failures (black box) and seismic profiles N2CH03 and 3D HR crossline 2839. The axis of the antiform is indicated (black dotted line). Note the occurrence of pockmarks along the channel-levee system and in the north-eastern part of the area. B) 3D HR crossline 2839 showing sub-surface structures at the top of the antiform, the fault network, and the UT/UH motif. C) Correlation map of the sea bottom showing the fault network and slides SA1, SA2 and SA3 indicated by dotted black lines. D) Correlation map of a horizon located at 100 ms twt below the base of the youngest UH (window = 128 ms twt). The sealing of most faults is well illustrated by comparing maps of correlation seismic attributes at the seabed (C), where only a few faults appear, and in the deeper subsurface, where numerous faults are visible (D). These faults (W-E oriented) are linked to the first compressive phase.

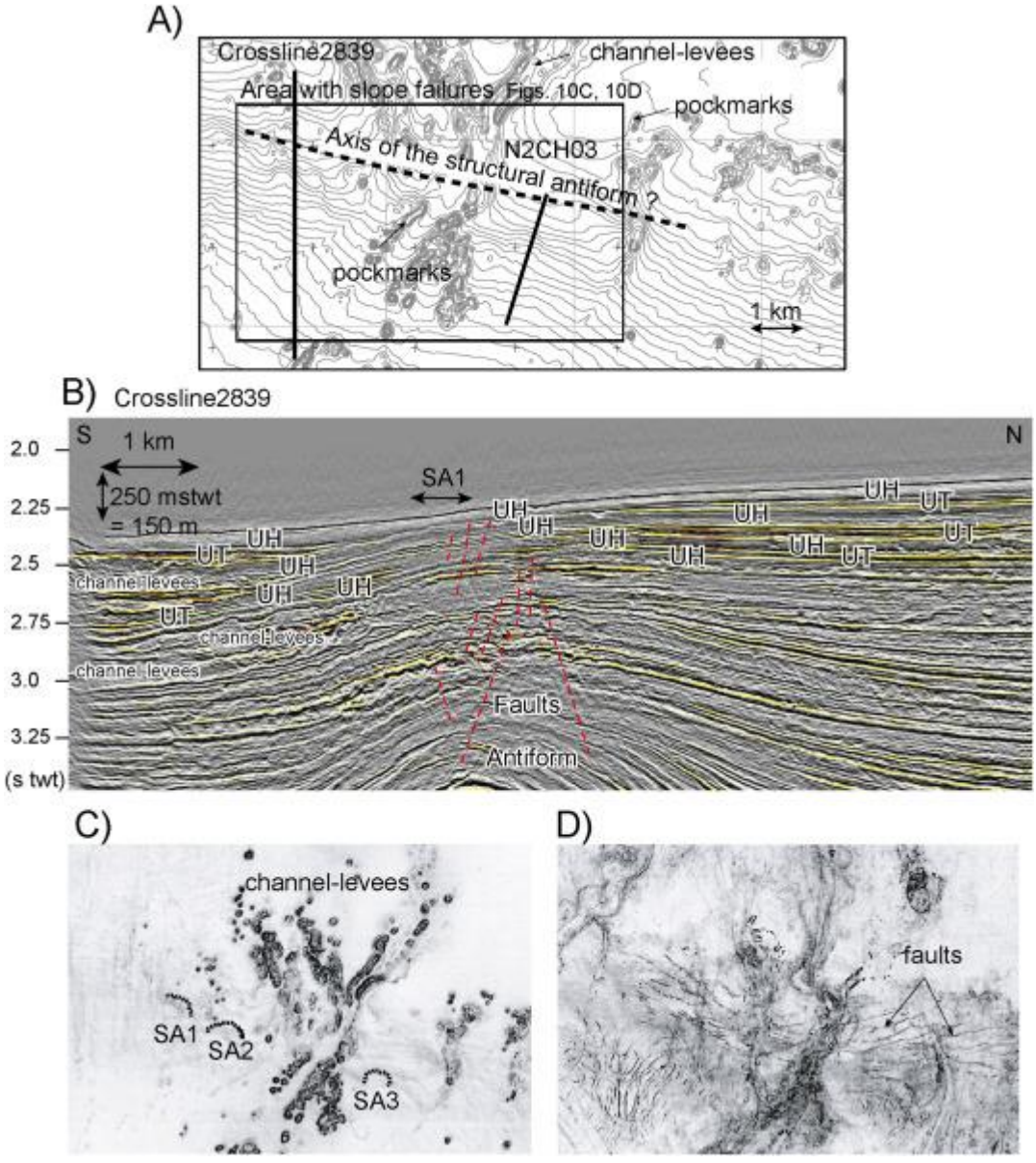

Fig. 11. Detailed internal structure of the area with slope failures. A) SYSIF profile N2CH03 showing slide SA3 (see Fig. 10A for orientation and location of N2CH3 and Fig. 10C for location of SA3). Note that only a few faults reach the seafloor at the head of the slide scar. Note the stacked UH units on the antiform top and the sub-units UH6 to UH1 (see zoom on the right). B) 3D HR line corresponding to SYSIF profile N2CH03 showing the deep anchoring of the fault network at the antiform top, the flat-shaped high-amplitude seismic anomalies of reflector R and channel-levees (CL) on the antiform flank.

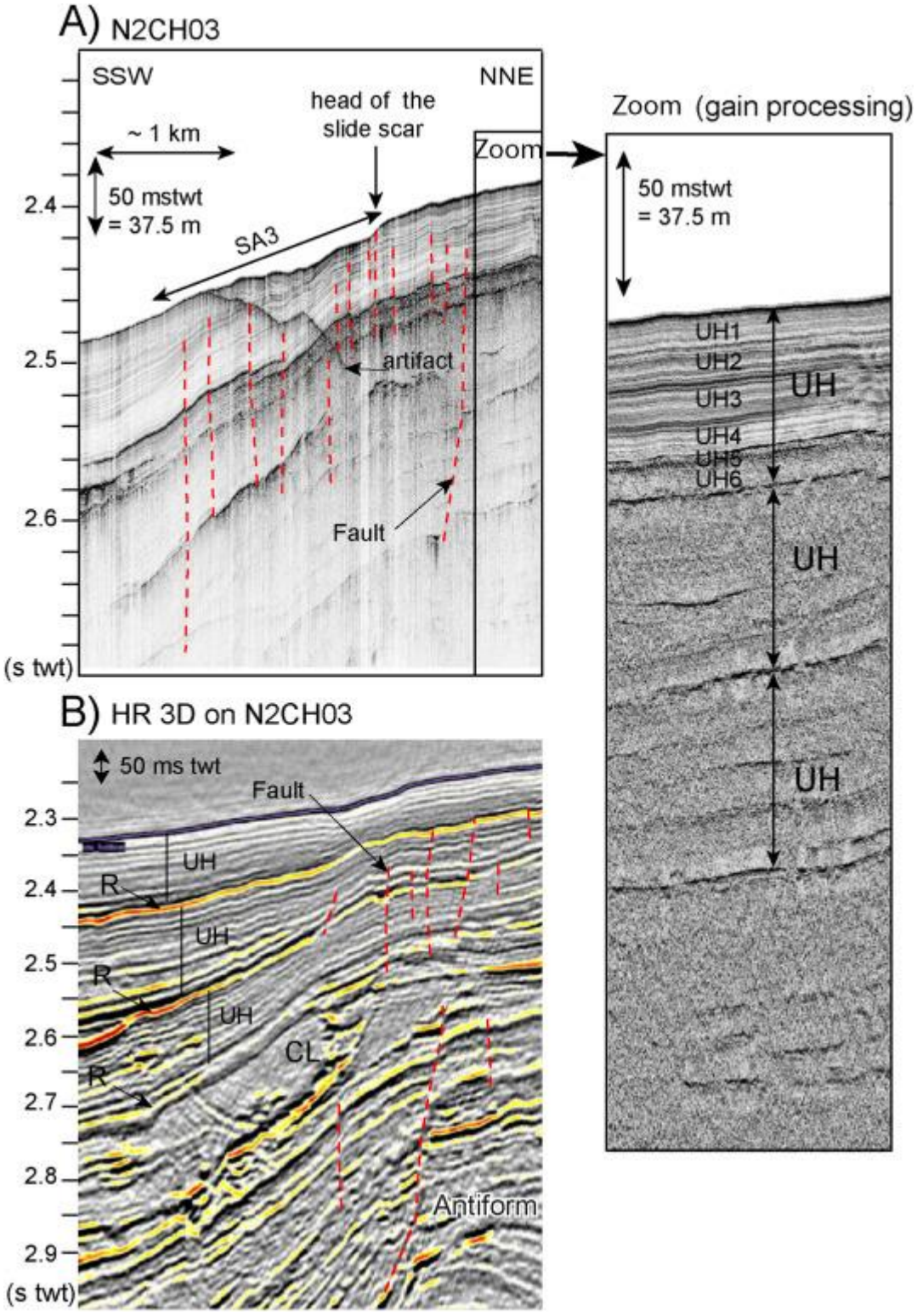

Fig. 12. Synthetic cartoon summarizing the three cold seep systems of the study region. The synthesis shows the underlying tectonic structure, the architecture of the plumbing systems and associated fluid flow seafloor features (the pockmark field previously studied by Marsset et al. (2018), the mud volcano and the area with living benthic fauna). Note the fault networks in structural antiforms and the underlying tectonic structures i.e. fold/thrust. Note the recurrence of fluid flow structures within UH units and sub-units UH6 to UH1 subunits i.e. at the scale of long- and short-term stratigraphic sequences described by Jermannaud et al. (2010). The deep and shallow fluid source layers are indicated.

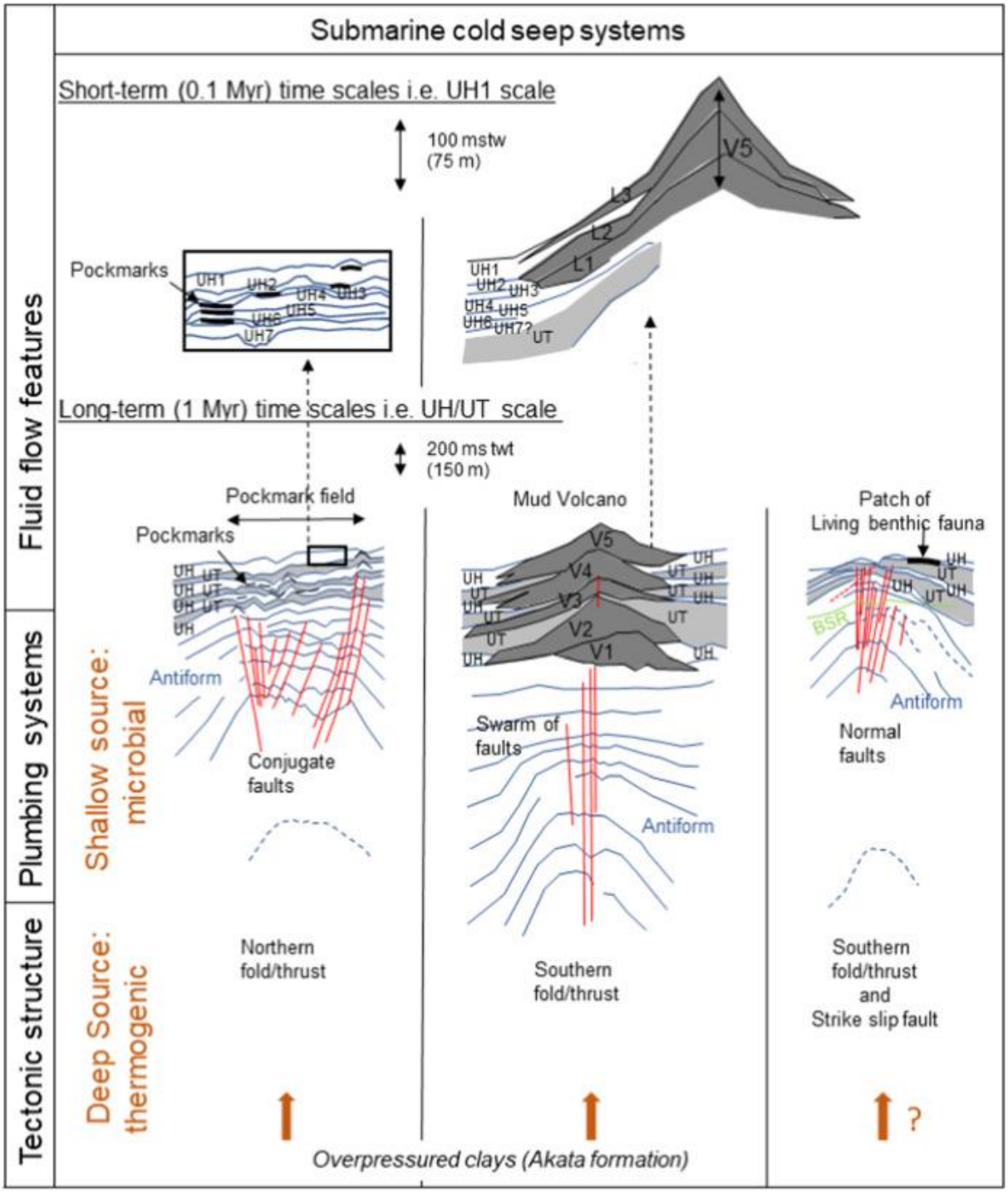

Fig. 13. Summary of controlling factors of fluid/gas migration activity in the eastern Niger Delta lobe on short- (0.1 Myr) time scale. Interpreted regional dip section (see Fig. 1, modified from Rouby et al., 2011) crossing the study region with superimposed controlling factors (MFS: Maximum Flooding Surface; UN5: Plio-Pleistocene sub-aerial unconformity; growth faults (thickened trace segments underline periods of major fluid flow activity)). Position of MeBo core GMMB01/02, located 3.5 km eastward is projected on the profile. Note the location of the study region in the transitional domain and the pockmark field above the northern thrust (see Fig. 3). Position of the strike-slip fault (SSF) (area with living benthic macrofauna 5 km westward) is indicated on the section (grey dotted lines) (Fig. 3). This diagram takes into consideration the geological context of the Niger Delta including its equatorial location i.e., effects of the monsoon, as well as gravity-driven deformation associated with underlying over-pressured shales and gas hydrate dynamics. It also integrates the concept of Catuneanu et al. (2019): “the rate of sedimentation at any specific location is controlled by all factors which modify sediment supply and the energy of the sediment-transport agents, including accommodation (subsidence +- eustasy), climate, source-area uplift, and autogenic processes that affect the pattern of sediment distribution within the basin”. The sediment supply was defined as the influx of sediment to the depositional area by the authors. The figure illustrates the architecture of the stratal pattern, which is controlled by two components: i) accommodation vertically and ii) sedimentation (sediment input to the ocean, sediment supply, and sedimentation rate) horizontally. The diagram integrates the variations of these two components depending on the glacial or interglacial period. These two components influence the generation of overpressure, the lithostatic load (sedimentation rate) and subsequent gravity-driven deformation that controls fluid/gas activity (seepage or not seepage). A) Glacial-interglacial transition and interglacial period correspond to a rise in sea-level and highstand, respectively, dominant clay-rich input, high sediment supply and high sedimentation rate on the slope and to a period of quiescence (no seepage). B) Interglacial-glacial transition and glacial period correspond to a drop in sea-level and lowstand, respectively, dominant siliciclastic sand-rich input, low sediment supply and low sedimentation rate on the slope. The gravity-driven deformation linked to sediment progradation and loading on the shelf during sea-level drop leads to generation of overpressure and lateral transmission of pressure. The relatively low hydrostatic pressure and low sedimentation rate on the slope during the lowstand favor seafloor fluid seeping.

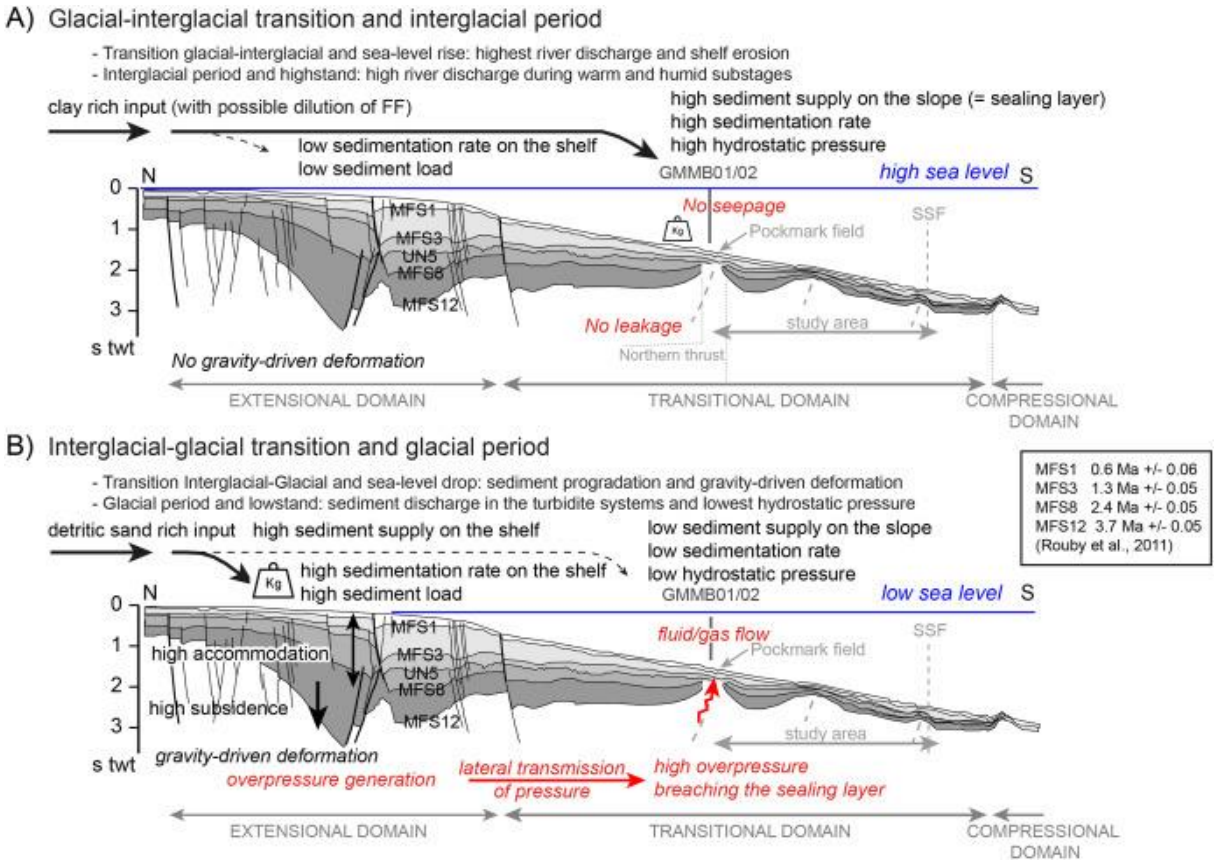

References

Allen, J.R.L., 1964. The Nigerian continental margin: bottom sediments, submarine morphology and geological evolution. Marine Geology 1, 289-332. https://doi.org/10.1016/0025-3227(64)90018-0.

Andreassen, K., Hubbard, A., Winsborrow, M., Patton, H., Vadakkepuliyambatta, S., Plaza-Faverola, A., Gudlaugsson, E., Serov, P., Deryabin, A., Mattingsdal, R., 2017. Massive blow-out craters formed by hydrate-controlled methane expulsion from the Arctic seafloor. Science, 356, 948-953. https://doi.org/10.1126/science.aal4500.

Andresen, K. J., Huuse, M., 2011. 'Bulls-eye' pockmarks and polygonal faulting in the Lower Congo Basin: Relative timing and implications for fluid expulsion during shallow burial, Marine Geology 279, 111-127. https://doi.org/10.1016/j.margeo.2010.10.016.

Armentrout, J. M., Kanschat, K.A., Meisling, K., Tsakma, J.J., Antrim, L., and McConnell, D.R., 2000. Neogene turbidite systems of the Gulf of Guinea continental margin slope,

offshore Nigeria. In: Bouma, A.H. and Stone, C.G. (Eds.), Fine Grained Turbidite Systems: American Association of Petroleum Geologists Memoir 72 and SEPM Special Publication 68, 93-108. https://doi.org/10.1306/M72703C9.

Armitage, S.J., Bristow, C.S., Drake, N.A, 2015. West African monsoon dynamics inferred from abrupt fluctuations of Lake Mega-Chad. Earth, Atmospheric, and Planetary Sciences 112, 8543-8548. https://doi.org/10.1073/pnas.1417655112.

Bailey, W., Shannon, P.M., Walsh, J.J., Unnithan, V., 2003. The spatial distributions of faults and deep sea carbonate mounds in the Porcupine Basin, offshore Ireland. Marine and Petroleum Geology 20, 509-522. https://doi.org/10.1016/S0264-8172(03)00079-5.

Bangs, N.L.B., Hornbach, M.J., Berndt, C., 2011. The mechanics of intermittent methane venting at South Hydrate Ridge inferred from 4D seismic surveying. Earth and Planetary Science Letters 310, 105-112, https://doi.org/10.1016/j.epsl.2011.06.022.

Bayon, G., Pierre, C., Etoubleau, J., Voisset, M., Cauquil, E., Marsset, T., Sultan, N., Le Drezen, E., Fouquet, Y., 2007. Sr/Ca and Mg/Ca ratios in Niger Delta sediments: implications for authigenic carbonate genesis in cold seep environments. Marine Geology 241, 93-109. https://doi.org/10.1016/j.margeo.2007.03.007.

Bayon, G., Henderson, G.M., Etoubleau, J., Caprais, J.C., Ruffine, L., Marsset, T., Dennielou, B., Cauquil, E., Voisset, M., Sultan, N., 2015. U-Th isotope constraints on gas hydrate and pockmark dynamics at the Niger delta margin. Marine Geology 370, 87-98. https://doi.org/10.1016/j.margeo.2015.10.012 1.

Bellingham, P., Connors, C., Haworth, R., Radovich, B., Danforth, A., 2014. The Deepwater Niger Delta: An Underexplored World Class Petroleum Province. GEOEXPRO 11, 1-9. https://archives.datapages.com/data/geo-expro-magazine/011/011005/pdfs/54.htm

Berndt, C., 2005. Focused fluid flow in passive continental margins. Philosophical Transactions of the Royal Society A 363, 2855-2871. https://doi.org/10.1098/rsta.2005.1666.

Berndt, C., Buenz, S., Mienert, J., 2003. Polygonal fault systems on the mid-Norwegian margin: a long-term source for fluid flow. In: Van Rensbergen, P., Hillis, R.R., Maltman,

A.J., Morley, C.K. (Eds.), Subsurface Sediment Mobilization. Geol. Soc. London Spec. Publ. 216, 283-290.

Bohrmann, G., Torres, M.E., 2014. Marine Gas Hydrates. In: Harff, J., Meschede, M., Petersen, S., Thiede, J. (Eds.), Encyclopedia of Marine Geosciences. Springer, Dordrecht. https://doi.org/10.1007/978-94-007-6644-0_168-2.

Bolton, A.J., Maltman, A.J., Clenell, M.B., 1998. The importance of overpressure timing and permeability evolution in fine-grained sediments undergoing shear. Journal of Structural Geology 20, 1013-1022. https://doi.org/10.1016/S0191-8141(98)00030-3.

Bonini, M., 2008. Elliptical mud volcano caldera as stress indicator in an active compressional setting (Nirano, Pede-Apennine margin, northern Italy). Geology 36, 131-134. https://doi.org/10.1130/G24158A.1.

Bonini, M., 2012. Mud volcanoes: indicators of stress orientation and tectonic controls. Earth Science Reviews 115, 121-152. https://doi.org/10.1016/j.earscirev.2012.09.002.

Briggs, S.E., Davies, R.J., Cartwright, J.A., Morgan, R., 2006. Multiple detachment levels and their control on fold styles in the compressional domain of the deepwater west Niger Delta. Basin Research 18, 435-450. https://doi.org/10.1111/j.1365-2117.2006.00300.

Briggs, S. E., Cartwright, J., Davies, R., 2009. Crustal structure of the deepwater west Niger Delta passive margin from the interpretation of seismic reflection data. Marine and Petroleum Geology 26, 936-950. https://doi.org/10.1016/j.marpe tgeo.2008.07.003.

Brooks, J.M., Bryant, W.R., Bernard, B.B., Cameron, N.R., 2000. The nature of gas hydrates on the Nigerian continental slope. Gas hydrates: challenges for the future. Annals of the New York Academy of Sciences 912, 76-93. https://doi.org/10.1111/j.1749-6632.2000.tb06761.x.

Burke, K., 1972. Longshore drift, submarine canyons, and submarine fans in developments of the Niger Delta. American Association of Petroleum Geologists Bull. 56, 1975-1983. https://doi.org/10.1306/819A41A2-16C5-11D7-8645000102C1865D.

Burke, K.C.B., Dessauvagie, T.F.J., Whiteman, A.J., 1971. The opening of the Gulf of Guinea and the geological history of the Benue Depression and the Niger Delta. Nature Physical Science 233, 51-55.

Caley, T., Malaizé, B., Revel, M., Ducassou, E., Wainer, K., Ibrahim, M., Shoeaib, D., Migeon, S., Marieu, V., 2011. Orbital timing of the Indian, East Asian and African boreal monsoons and the concept of a 'global monsoon'. Quaternary Science Reviews 30, 3705-3715. https://doi.org/10.1016/j.quascirev.2011.09.015.

Cathles, L.M., Su, Z. and Chen, D., 2010. The physics of gas chimney and pockmarks formation, with implications for assessment of seafloor hazards and gas sequestration. Marine and Petroleum Geology 27, 82-91. https://doi.org/10.1016/j.marpetgeo.2009.09.010.

Catuneanu, O., 2019. Model-independent sequence stratigraphy. Earth-Science Reviews 188, 312-388. https://doi.org/10.1016/j.earscirev.2018.09.017.

Chenrai, P., Huuse, M., 2017. Pockmark formation by porewater expulsion during rapid progradation in the offshore Taranaki Basin, New Zealand. Marine and Petroleum Geology 82, 399-413. https://doi.org/10.1016/j.marpetgeo.2017.02.017.

Chima, K.I., Do Couto, D., Leroux, E., Gardin, S., Hoggmasacall, N., Rabineau, M., Granjean, D., Gorini, C., 2019. Seismic stratigraphy and depositional architecture of Neogene intraslope basins, offshore western Niger Delta. Marine and Petroleum Geology 109, 449-468. https://doi.org/10.1016/j.marpetgeo.2019.06.030.

Chima, K. I., Gorini, C., Rabineau, M., Granjeon, D., Do Couto, D., Leroux, E., Gardin, S., Hoggmasacall, N., 2020. Pliocene and Pleistocene stratigraphic evolution of the western Niger Delta intraslope basins: A record of glacio-eustatic sea-level and basin tectonic forcings. Global and Planetary Change 195, 103355. https://doi.org/10.1016/j.gloplacha.2020.103355.

Chima, K. I., Granjeon, D., Do Couto, D., Leroux, E., Gorini, C., Rabineau, M., Letouzey, J., Hoggmasacall, N., Glukstad, M.M., 2021. Tectono-stratigraphic evolution of the offshore western Niger Delta from the Cretaceous-present: Implication of delta

dynamics and paleo-topography on gravity-driven deformation. Basin Research. https://doi.org/10.1111/bre.12609.

Cobbold, P.R., Clarke, B.J., Løseth, H., 2009. Structural consequences of fluid overpressure and seepage forces in the outer thrust belt of the Niger Delta. Petroleum Geoscience 15, 3-15. https://doi.org/10.1144/1354-079309-784.

Cole, J.M., Goldstein, S.L., de Menocal, P.B., Hemming, S.R., Grousset, F.E., 2009. Contrasting compositions of Saharan dust in the eastern Atlantic Ocean during the last deglaciation and African Humid Period. Earth and Planetary Science Letters 278, 257-266. https://doi.org/10.1016/j.epsl.2008.12.011.

Collins, J.A., Schefuß, E., Govin, A., Mulitza, S., Tiedemann, R., 2014. Insolation and glacial-interglacial control on southwestern African Hydroclimate over the last 140,000 years. Earth and Planetary Science Letters 398, 1-10. https://doi.org/1016/j.epsl.2014.04.034. hal-02180974.

Constantinescu, A.M., Toucanne, S., Dennielou, B., Jorry, S.J., Mulder, T. and Lericolais, G., 2015. Evolution of the danube deep-sea fan since the last glacial maximum: New insights into Black Sea water-level fluctuations. Marine Geology 367, 50-68. https://doi.org/10.1016/j.margeo.2015.05.007.

Corredor, F., Shaw, J.H., Bilotti F., 2005. Structural styles in the deep-water fold and thrust belts of the Niger Delta. American Association of Petroleum Geologists Bull. 89, 753-780. https://doi.org/10.1306/02170504074.

Croudace, I.W., Rindby, A., Rothwell, R.G., 2006. ITRAX: description and evaluation of a new multi-function X-ray core scanner. Geological Society, London, Special Publications, 267, 51-63, 1. https://doi.org/10.1144/GSL.SP.2006.267.01.04.

Cunningham, R., Lindholm, R.M., 2000. Seismic evidence for wide extruded mud flows gas hydrate formation, Offshore West Africa. In: Mello, M.R., Katz, B.J. (Eds.), Petroleum systems of South Atlantic margins. American Association of Petroleum Geologists Memoir 73, 93-105.

Damuth, J.E., 1994. Neogene gravity tectonics and depositional processes on the deep Niger Delta continental margin. Marine and Petroleum Geology 11, 320-346. https://doi.org/10.1016/0264-8172(94)90053-1.

Darnell, K.N., Flemings, P.B., 2015. Transient seafloor venting on continental slopes from warming-induced methane hydrate dissociation. Geophysical Research Letters 42, 765-10, 772. https://doi.org/10.1002/2015GL067012.

Davy, B., Pecher, I., Wood, R., Carter, L., Gohl, K., 2010. Gas escape features off New Zealand: Evidence of massive release of methane from hydrates. Geophysical Research Letters 37. https://doi.org/10.1029/2010gl045184.

Dean, J.F., 2020. Old methane and modern climate change. Science 367, 846-848. https://doi.org/10.1126/science.aba8518.

De Menocal, P.B., 1995. Plio-Pleistocene African Climate: Science 270, 53-59. https://doi.org/10.1126/science.270.5233.53.

De Menocal, P.B., Ortiz, J., Guilderson, T., Adkins, J., Sarnthein, M., Baker, L., Yarusinsky, M., 2000. Abrupt onset and termination of the African Humid Period: rapid climate responses to gradual insolation forcing. Quaternary Science Reviews 19, 347-361. https://doi.org/10.1016/S0277-3791(99)00081-5.

de Prunelé, A., Ruffine, L., Riboulot, V., Peters, C.A., Guyader, V., Carnavallo, L., Bayon, G., Donval, J.P., Sultan, N., Caprais, J.C., Marsset, T., Pape, T., Bohrmann, G., Géli, L., Lescanne, M., Cauquil, E., 2017. Focused hydrocarbon-migration in shallow sediments of a pockmark cluster in the Niger Delta (Off Nigeria). Geochemistry, Geophysics, Geosystems 18. https://doi.org/10.1002/2016GC006554.

Deville, E., Guerlais, S.H, Lallemant, F., Schneider, F., 2010. Fluid dynamics and subsurface sediment mobilization processes: an overview from Southeast Caribbean. Basin Research 22, 361-379. https://doi.org/10.1111/j.1365-2117.2010.00474.x.

Dewangan, P., Ramprasad, T., Ramana, M.V., Mazumdar, A., Desa, M., Badesab, F.K., 2010. Seabed morphology and gas venting features in the continental slope region of Krishnae Godavari basin, Bay of Bengal: Implications in gas-hydrate exploration.

Marine and Petroleum Geology 27, 1628-1641. https://doi.org/10.1016/j.marpetgeo.2010.03.015.

Doust, H., Omatsola, E., 1990. Niger Delta. In: Edwards, J.D., Santogrossi, P.A. (Eds.), Divergent/passive margin basins. American Association of Petroleum Geologists Memoir 48, 201-238.

Ducassou, E., Migeon, S., Mulder, T., Murat, A., Capotondi, L., Bernasconi, S.M., Mascle, J., 2009. Evolution of the Nile deep-sea turbidite system during the late Quaternary: influence of climate change on fan sedimentation. Sedimentology 56, 2061-2090. https://doi.org/10.1111/j.1365-3091.2009.01070.x.

Dugan, B., Flemings, P., Olgaard, D.L., Gooch, M.J., 2003. Consolidation, effective stress, and fluid pressure of sediments from ODP Site 1073, US mid-Atlantic continental slope. Earth and Planetary Science Letters 215, 13-26. https://doi.org/ 10.1016/S0012-821X(03)00425-4.

Dumke, I., Berndt, C., Crutchley, G.J., Krause, S., Liebetrau, V., Gay, A., Couillard, M., 2014. Seal bypass at the Giant Gjallar Vent (Norvegian Sea): Indications for a new phase of fluid venting at a 56-Ma-old fluid migration system. Marine Geology 351, 38-52. https://doi.org/10.1016/j.margeo.2014.03.006.

Dupont, L.M., Donner, B., Schneider, R., Wefer, G., 2001. Mid-Pleistocene environmental change in tropical Africa began as early as 1.05 Marine Geology 29, 195-198. https://doi.org/10.1130/0091-7613(2001)029<0195:MPECIT>2.0.CO;2.

Dypvik, H., Harris, N.B., 2001. Geochemical facies analysis of fine-grained siliciclastics using Th/U, Zr/Rb and (Zr+ Rb)/Sr ratios. Chemical Geology 181, 131-146. https://doi.org/10.1016/S0009-2541(01)00278-9.

Etiope, G., Ciotoli, G., Schwietzke, S., Schoell, M., 2019. Gridded maps of geological methane emissions and their isotopic signature. Earth System Science Data. https://doi.org/10.5194/essd-11-1-2019.

Evamy, B.D., Haremboure, J., Kamerling, P., Knapp, W., Molloy, F.A., Rowlands, P.H., 1978. Hydrocarbon habitat of Tertiary Niger Delta. American Association of Petroleum Geologists Bull. 62, 1-39. https://doi.org/10.4236/ojg.2021.115009.

Feng, D., Qiu, J.W., Hu, Y., Peckmann, J., Guan, H., Tong, H., Chen, C., Chen, J., Gong, S., Li, N., Chen, D., 2018. Cold seep systems in the South China Sea: An overview. Journal of Asian Earth Sciences 168, 3-16. https://doi.org/10.1016/j.jseaes.2018.09.021.

Foschi, M., Cartwright, J.A., 2016. South Malvinas/Falkland Basin: Hydrocarbon migration and petroleum system. Marine and Petroleum Geology 77, 124-140. https://doi.org/10.1016/J.MARPETGEO.2016.06.002.

Foschi, M., Cartwright, J.A., MacMinn, C.W., Etiope, G., 2020. Evidence for massive emission of methane from a deep-water gas field during the Pliocene. Earth, Atmospheric, and Planetary Sciences 117, 27869-27876. https://doi.org/10.1073/pnas.2001904117.

Foucher, J.P., Nouze, H., Henry, P., 2002. Observation and tentative interpretation of a double BSR on the Nankai slope. Marine Geology 187, 161-175. https://doi.org/10.1016/S0025-3227(02)00265-7.

Freudenthal, T., Wefer, G., 2013. Drilling cores on the sea floor with the remote-controlled sea floor drilling rig MeBo. Geoscientific Instrumentation Methods and Data Systems 2, 329-337. https://doi.org/10.5194/gi-2-329-2013.

Garziglia, S., 2010. Typologie, phénoménologie et approche des facteurs déclenchants des glissements sous-marins : application aux deltas profonds du Nil et du Niger. PhD thesis. Université Nice-Sophia Antipolis, p. 371. https://www.theses.fr/2010NICE4112

Gay, A., Lopez, M., Berndt, C., Séranne, M., 2007. Geological controls on focused fluid flow associated with seafloor seeps in the Lower Congo Basin. Marine Geology 244, 68-92. https://doi.org/10.1016/j.margeo.2007.06.003.

Gay, A., Cavailhes, T., Grauls, D., Marsset, B., Marsset, T., 2017. Repeated fluid expulsions during events of rapid sea-level rise in the Gulf of Lion, western Mediterranean Sea.

Bulletin de la Société Geologique de France, 188, 24. https://doi.org/10.1051/bsgf/2017190.

George, R.A., Cauquil, E., 2007. AUV ultrahigh-resolution 3D seismic technique for detailed subsurface investigations. In: Offshore Technology Conference. Houston, TX, USA. OTC 18784. https://doi.org/10.4043/18784-MS

Govin, A., Varma, V., Prange, M., 2014. Astronomically forced variations in western African rainfall (21°N-20°S) during the Last Interglacial period. Geophysical Research Letters 41, 2117-2125. https://doi.org/10.1002/2013GL058999.

Graue, K., 2000. Mud volcanoes in deepwater Nigeria. Marine and Petroleum Geology 17, 959-974. https://doi.org/10.1016/S0264-8172(00)00016-7.

Gutierrez Parades, H.C., Catuneanu, O., Romano, U.H., 2017. Sequence stratigraphy of the Miocene section, southern Gulf of Mexico. Marine and Petroleum Geology 86, 711-732.

Haskell, N., Nissen, S., Hughes, M., Grindhaug, J., Dhanani, S., Heath, R., Kantorowicz, J., Antrim, L., Cubanski, M., Nataraj, R., Schilly, M., Wigger, S., 1999. Delineation of geologic drilling hazards using 3-D seismic attributes. The leading edge 18, 373-382. https://doi.org/10.1190/1.1438301.

Heggland, R., 2003. Vertical Hydrocarbon Migration at the Nigerian Continental Slope: Applications of Seismic Mapping Techniques. American Association of Petroleum Geologists Annual Convention, Salt Lake City, May 11-14. https://www.searchanddiscovery.com/pdfz/abstracts/pdf/2003/annual/extend/ndx_79203.PDF.html

Heggland, R., Hovland, M., Graue, K., Gallagher, J.W., 2001. Mud volcanoes and gas hydrates on the Niger Delta Front. In: Conference Abstract Book: Subsurface Sediment Mobilization. University of Gent, Belgium. Sept, 44. https://www.researchgate.net/publication/262648118_Mud_volcanoes_and_gas_hydrates_on_the_Niger_Delta_front

Hooper, R.J., Fitzsimmons, R.J., Grant, N., Vendeville, B.C., 2002. The role of deformation in controlling depositional patterns in the south-central Niger Delta, West Africa. Journal of Structural Geology 24, 847-859. https://doi.org/10.1016/S0191-8141(01)00122-5.

Hovland, M., Gallagher, J.W., Clennell, M.B., Lekvam K., 1997. Gas hydrate and free gas volumes in marine sediments: example from the Niger Delta front. Marine and Petroleum Geology 14 , 245-255.

Hovland, M., Heggland, R., De Vries, M.H. and Tjelta, T.I., 2010. Unit-pockmarks and their potential significance for predicting fluid flow. Marine and Petroleum Geology 27, 1190-1199. https://doi.org/10.1016/j.marpetgeo.2010.02.005.

Jahn, B., Schneider, R.R., Müller, P.J., Donner, B. and Röhl, U., 2005. Response of tropical African and East Atlantic climates to orbital forcing over the last 1.7 Ma. In: Head, M.J., Gibbard, P.L. (Eds.), Early-Middle Pleistocene Transitions: The Land-Ocean Evidence: Geological Society, London, Special Publications 247, 65-84. https://doi.org/10.1144/GSL.SP.2005.247.01.04.

Jermannaud, P., Rouby, D., Robin, C., Nalpas, T., Guillocheau, F., Raillard, S., 2010. Plio-Pleistocene sequence stratigraphic architecture of the eastern Niger Delta: a record of eustasy and aridification of Africa. Marine and Petroleum Geology 27, 810-821. https://doi.org/10.1016/j.marpetgeo.2009.12.005.

Jobe, Z.R., Sylvester, Z., Parker, A.O., Howes, N., Slowey, N., and Pirmez, C., 2015. Rapid adjustment of submarine channel architecture to changes in sediment supply: Journal of Sedimentary Research 85, 729-753. https://doi.org/10.2110/jsr.2015.30.

Jolly, B. A., Lonergan, L., Whittaker, A. C., 2016. Growth history of fault-related folds and interaction with seabed channels in the toe-thrust region of the deep-water Niger Delta. Marine and Petroleum Geology 70, 58-76. https://doi.org/10.1016/j.marpetgeo.2015.11.003.

Judd, A., Hovland, M., 2009. Seabed Fluid Flow: The Impact on Geology, Biology and the Marine Environment. Cambridge University Press. https://doi.org/10.1017/CBO9780511535918.

Kallweit, W., Mollenhauer, G., Zabel, M., 2012. Multi-proxy reconstruction of terrigenous input and sea-surface temperatures in the eastern Gulf of Guinea over the last ~35 ka. Marine Geology 319-322, 35-46. https://doi.org/10.1016/j.margeo.2012.06.007.

Karaket, A., Chenrai, P., Huuse, M., 2021. Seismic Characteristics of Paleo-Pockmarks in the Great South Basin, New Zealand. Frontiers in Earth Science 9, 623. https://doi.org/10.3389/feart.2021.683617.

Katz B.J. and Dempster K., 2003. Hydrocarbon Charge in Deepwater Nigeria - An Evolving Story. American Association of Petroleum Geologists International Conference Barcelona, Spain, September 21-24, 2003. https://www.searchanddiscovery.com/pdfz/abstracts/pdf/2003/intl/short/ndx_83728.pdf.html.

Kennett, J.P., Cannariat, K.G., Hendy, I.L., Behl, R.J., 2000. Carbon isotopic evidence for methane hydrate instability during Quaternary Interstitials. Science 288, 128-133. https://doi.org/10.1126/science.288.5463.12.

Ker, S., Marsset, B., Garziglia, S., Le Gonidec, Y., Gibert, D., Voisset, M., Adamy, J., 2010. High-resolution seismic imaging in deep sea from a joint deep-towed/OBH reflection experiment: application to a Mass Transport Complex offshore Nigeria. Geophysical Journal 182, 1524-1542. https://doi.org/10.1111/j.1365-246X.2010.04700.x.

Knox, G.J., Omatsola, E.M., 1989. Development of the Cenozoic Niger delta in terms of the “escalator regression” model and impact on hydrocarbon distribution. Koninklijk Nederlands Geologisch en Mijnbouwkundig Gezelschap Symposium on Coastal Lowlands, Geology and Geotechnology Proceeding (1987). Kluwer Academic Publishers, Dortrecht, Netherlands, 181-202. https://doi.org/10.1007/978-94-017-1064-0_12.

Kopf, A.J., 2002. Significance of mud volcanism. Review of Geophysics 40, 1-52. https://doi :10.1029/2000RG000093.

https://doi.org/10.1038/ngeo256.

Lafuerza, S., Sultan, N., Canals, M., Frigola, J., Berné, S., Jouet, G., Galavazi, M., and Sierro, F.J., 2009. Over-pressure within upper continental slope sediments from CPTU data, Gulf of Lion, NW Mediterranean Sea. International Journal of Earth Sciences, 98, 751-768, https://doi.org/10.1007/s00531-008-0376-2.

Laurent, D., Marsset, T., Droz, L., Granjeon, D., Molliex, S., Picot, M., Rabineau, M., 2020. 4D forward stratigraphic modelling of the Late Quaternary Congo deep-sea fan: Role of climate/vegetation coupling in architectural evolution. Marine Geology 429, 106334. https://doi.org/10.1016/j.margeo.2020.106334.

Leduc, A.M., Davies, R.J., Swarbrick, R.E, Imber, J., 2013. Fluid flow pipes triggered by lateral pressure transfer in the deepwater western Niger Delta. Marine and Petroleum Geology 43, 423-433. https://doi.org/10.1016/j.marpetgeo.2012.12.005.

Lehner, P., De Ruiter, P.A.C., 1977. Structural history of Atlantic Margin of Africa: American Association of Petroleum Geologists Bull. 61, 961-981. https://doi.org/10.1306/C1EA43B0-16C9-11D7-8645000102C1865D.

Lezine, A.-M., Cazet, J.-P., 2005. High-resolution pollen record from core KW31, Gulf of Guinea, documents the history of the lowland forests of West Equatorial Africa since 40,000 yr ago. Quaternary Research 64, 432-443. https://doi.org/10.1016/j.yqres.2005.08.007.

Lézine, A.-M., Duplessy, J.-C., Cazet, J.-P., 2005. West African monsoon variability during the last deglaciation and the holocene: Evidence from fresh water algae, pollen and isotope data from Core KW31, Gulf of Guinea. Palaeogeography, Palaeoclimatology Palaeoecology 219 (3-4), 225-237. https://doi.org/10.1016/j.palaeo.2004.12.027.

Lézine, A.-M., Bassinot, F., Peterschmitt, J.-Y., 2014. Orbitally-induced changes of the Atlantic and Indian monsoons over the past 20,000 years: New insights based on the comparison of continental and marine records. Bulletin De La Société Géologique De France 185, 3-12. https://doi.org/10.2113/GSSGFBULL.185.1.3.

Lisiecki, L.E., Raymo, M.E., 2005. A Pliocene-pleistocene stack of 57 globally distributed benthic δ18O records. Paleoceanography 20, PA1003. https://doi.org/10.1029/2004PA001071.

Lombo Tombo, S., Dennielou, B., Berné, S., Bassetti, M.A., Toucanne, S., Jorry, S.J., Jouet, G., Fontanier, C., 2015. Sea-level control on turbidite activity in the Rhone canyon and the upper fan during the Last Glacial Maximum and Early deglacial. Sedimentary Geology 323, 148-166. https://doi.org/10.1016/j.sedgeo.2015.04.009.

Løseth, H., Wensaas, L., Arntsen, B., Hanken, N.M., Basire, C., Graue, K., 2011. 1000 m long gas blow-out pipes. Marine and Petroleum Geology 28, 1047-1060. https://doi.org/10.1016/j.marpetgeo.2010.10.001.

Ma, G., Zhan, L., Lu, H., Hou, G., 2021. Structures in 932 Shallow Marine Sediments Associated with Gas and Fluid Migration. Journal of Marine Science And Engineering 9, 396. https://doi.org/10.3390/jmse9040396.

McArthur, J. M., Howarth, R.J., Shields, G.A., 2012. Strontium Isotope Stratigraphy. In: Gredstein, F.M, Ogg, J.G., Schmotz, M.D. Ogg, G.M. (Eds.), The Geologic Time Scale. Boston, Elsevier, 127-144.Maestrelli, D., Iacopini, D., Jihad, A.A., Bond, C.E., Bonini, M., 2017. Seismic and structural characterization of fluid escape pipes using 3D and partial stack seismic from the Loyal Field (Scotland, UK): A multiphase and repeated intrusive mechanism. Marine and Petroleum Geology 88, 489-510. https://doi.org/10.1016/j.marpetgeo.2017.08.016.

Magara, K., 1978. Compaction and fluid migration. Practical petroleum geology. Developments in Petroleum Science 9, Elsevier Amsterdam, pp 319. https://www.sciencedirect.com/bookseries/developments-in-petroleum-science/vol/9/suppl/C

Maley, J., Brenac, P., 1998. Vegetation dynamics, palaeoenvironments and climatic change in the forests of western Cameroon during the last 28000 years BP. Review of Palaeobotany and Palynology 99, 157-187. https://doi.org/10.1016/S0034-6667(97)00047-X.

Maltman, A., Bolton, A., 2003. How sediment become mobilized. In: Van Rensbergen, P., Hillis, R.R., Maltman, A.J., Morley, C.K. (Eds.), Subsurface Sediment Mobilization. Geol. Soc. London Spec. Publ. 216, 9-20.

Marsset, T., Marsset, B., Ker, S., Thomas, Y., Le Gall, Y., 2010. High and very high resolution deep-towed seismic system: performance and examples from deep water geohazard studies. Deep Sea Research I 57, 628-637. https://doi.org/10.1016/j.dsr.2010.01.001.

Marsset, T., Ruffine, L., Gay, A., Ker, S., Cauquil, E. 2018. Types of fluid-related features controlled by sedimentary cycles and fault network in deepwater Nigeria. Marine and Petroleum Geology 89, 330-349. https://doi.org/10.1016/j.marpetgeo.2017.10.004.

Mazzini, A., Svensen, H.H., Forsberg, C.F., Linge, H, Lauritzen, S.E., Haflidason, H., Hammer, Ø., Planke, S., Tjelta, T.I., 2017. A climatic trigger for the giant Troll pockmark field in the northern North Sea. Earth and Planetary Science Letters 464, 24-34. https://doi.org/10.1016/j.epsl.2017.02.014.

Medialdea, T., Somoza, L., Pinheiro, L.M., Fernández-Puga, M.C., Vázquez, J.T., León, R., Ivanov, M.K., Magalhaes, V., Díaz-del-Río, V., Vegas, R., 2008. Tectonics and mud volcano development in the Gulf of Cádiz. Marine Geology 26, 1-4, 48-63. https://doi.org/10.1016/j.margeo.2008.10.007.

Mikkelsen, N., Maslin, M., Giraudeau, J. and Showers, J.W., 1997. Biostratigraphy and sedimentation rates on the Amazon fan. In: Flood, R.D., Piper, D.J.W., Klaus, A., Peterson, L.C. (Eds.), Proceedings of the Ocean Drilling Program, Scientific Results, 155, 577-594. https://doi.org/10.2973/odp.proc.sr.155.248.1997.

Milkov, A.V., 2000. Worldwide distribution of submarine mud volcanoes and associated gas hydrates. Marine Geology 167, 29-42. https://doi.org/10.1016/S0025-3227(00)00022-0.

Morley, C.K., Guerin, G., 1996. Comparison of gravity driven deformation styles and behaviour associated with mobile shales and salt. Tectonics 15, 1154-1170. https://doi.org/10.1029/96TC01416.

Mourgues, R., Lecomte, E., Vendeville, B., Raillard, S., 2009. An experimental investigation of shale tectonics in progradationnal delta. Tectonophysics 474, 643–656.

Nimblett, J., Ruppel, C., 2003. Permeability evolution during the formation of gas hydrates in marine sediments. Journal of Geophysical Research: Solid Earth 108 . https://doi.org/10.1029/2001JB001650.

Niyazi, Y., Eruteya, O.E., Maitituerdi, A., Warne, M., Ierodiaconou, D., 2022. First evidence of (Paleo)pockmarks in the Bass Strait, offshore SE Australia: A forced regression modulated shallow plumbing system, Marine and Petroleum Geology 142, 105749. https://doi.org/10.1016/j.marpetgeo.2022.105749.

Olabode, S.O., Adekoya, J.A. 2008. Seismic stratigraphy and development of Avon canyon in Benin (Dahomey) basin, southwestern Nigeria. Journal of African Earth Sciences 50, 286-304. https://doi.org/10.1016/j.jafrearsci.2007.10.002.

Osborne, M.J., Swarbrick, R.E., 1997. Mechanisms for generating overpressure in sedimentary basins: a reevaluation. American Association of Petroleum Geologists Bull. 81, 1023-1041.

Paganoni, M., Cartwright, J.A., Foschi, M., Shipp, C.R., Van Rensbergen, P., 2018. Relationship between fluid-escape pipes and hydrate distribution in offshore Sabah (NW Borneo). Marine Geology 395, 82-103. https://doi.org/10.1016/j.margeo.2017.09.010.

Pape, T., Ruffine, L., Hong, W.-L., Sultan, N., Riboulot, V., Peters, C.A., Kölling, M., Zabel, M., Garziglia, S., Bohrmann, G., 2020. Shallow gas hydrate accumulations at a Nigerian deepwater pockmark - Quantities and dynamics. Journal of Geophysical Research: Solid Earth 125 . https://doi.org/10.1029/2019jb018283.

Pasquier, V., Revillon, S., Leroux, E., Molliex, S., Moccochain, L., Rabineau, M., 2019. Quantifying Biogenic Versus Detrital Carbonates on Marine Shelf: An Isotopic Approach. Frontiers in Earth Science 7:164. https://doi.org/10.3389/feart.2019.00164.

Pastouret L., Chamley H., Delibrias G., Duplessy J.C., Thiede J., 1978. Late quaternary climatic changes in western tropical africa deduced from deep-sea sedimentation off

the Niger delta. Oceanologica Acta, 1(2), 217-232.: https://archimer.ifremer.fr/doc/00000/5227/.

Pennino, V., Sulli, A., Caracausi, A., Grassa, F., Interbartolo, F., 2014. Fluid escape structures in the north Sicily continental margin. Marine and Petroleum Geology 55, 202-213. https://doi.org/10.1016/j.marpetgeo.2014.02.007.

Phrampus, B.J., Hornbach, M.J., 2012. Recent changes to the Gulf Stream causing widespread gas hydrate destabilization. Nature 490, 527-530. https://doi.org/10.1038/nature11528.

Picot, M., 2015. Cycles sédimentaires dans le système turbiditique du Congo: nature et origine. PhD Thesis. University of Brest (UBO), 368 pp. https://archimer.ifremer.fr/doc/00312/42275/

Picot, M., Marsset, T., Droz, L., Dennielou, B., Baudin, F., Hermoso, M., De Rafelis, M., Sionneau, T., Cremer, M., Laurent, D., Bez, M., 2019. Monsoon control on channel avulsions in the Late Quaternary Congo Fan. Quaternary Science Reviews 204, 149-171.

Pinheiro, L.M., Magalhães, V., Somoza, L., Gardner, J., Ivanov, M., Kopf, A., Rensbergen, P.V., Monteiro, J.H., Euromargins-MVSEIS Team, 2006. Structural control of mud volcanism and hydrocarbon-rich fluid seepage in the Gulf of Cádiz: recent results from the TTR-15 cruise. In: Mascle, J., Sakellariou, D., Briand, F. (Eds.), Fluid Seepages/Mud Volcanoes in the Mediterranean and Adjacent Domains. CIESM Workshop Monographs 29, 53-58. Monaco.

Plaza-Faverola, A., Bünz, S., Mienert, J., 2011. Repeated fluid expulsion through sub-seabed chimneys offshore Norway in response to glacial cycles, Earth and Planetary Science Letters 305, 297-308, https://doi.org/10.1016/j.epsl.2011.03.001.

Plaza-Faverola, A., Vadakkepuliyambatta, S., Hong, W.-L., Mienert, J., Bünz, S., Chand, S., Greinert, J., 2017. Bottom-simulating reflector dynamics at Arctic thermogenic gas provinces: An example from Vestnesa Ridge, offshore west Svalbard. Journal of

Geophysical Research: Solid Earth 122, 4089-4105, https://doi.org/10.1002/2016JB013761.

Pokras, E.M., 1987. Diatom record of late Quaternary climatic change in the eastern equatorial Atlantic and tropical Africa. Paleoceanography 2, 273-286. https://doi.org/10.1029/PA002i003p00273.

Portnov, A., Vadakkepuliyambatta, S., Mienert, J., Hubbard, A., 2016. Ice-sheet-driven methane storage and release in the Arctic. Nature Communication 7, 10314. https://doi.org/10.1038/ncomms10314.

Riboulot, V., 2011. Facteurs de contrôle du fonctionnement des pockmarks durant les derniers cycles climatiques (Partie orientale du delta sous-marin du Niger et Golfe du Lion), PhD thesis, Université of Perpignan, France, 243 pp.

Riboulot, V., Cattaneo, A., Berné, S., Schneider, R.R., Voisset, M., Imbert, P., Grimaud, S., 2012. Geometry and chronology of late Quaternary depositional sequences in the Eastern Niger Submarine Delta. Marine Geology 319-322, 1-20. https://doi.org/10.1016/j.margeo.2012.03.002.

Riboulot, V., Cattaneo, A., Sultan, N., Garziglia, S., Ker, S., Imbert, P., Voisset, M., 2013. Sea-level change and free gas occurrence influencing a submarine landslide and pockmark formation and distribution in deepwater Nigeria. Earth and Planetary Science Letters 375, 78-91. https://doi.org/10.1016/j.epsl.2013.05.013.

Riboulot, V., Ker, S., Sultan, N., Thomas, Y., Marsset, B., Scalabrin, C., Ruffine, L., Boulart, C., Ion, G., 2018. Freshwater lake to salt-water sea causing widespread hydrate dissociation in the Black Sea, Nat. Commun. 9:117. https://doi.org/10.1038/s41467-017-02271-z

Richter, T.O., van der Gaast, S., Koster, B., Vaars, A., Gieles, R., de Stigter, H.C., De Haas, H., van Weering, T.C.E., 2006. Geological Society, London, Special Publications 267, 39-50, 1. The Avaatech XRF Core Scanner: technical description and applications to NE Atlantic sediments. https://doi.org/10.1144/GSL.SP.2006.267.01.03.

Rongemaille, E., Bayon, G., Pierre, C., Bollinger, C., Chu, N.C., Fouquet, Y., Riboulot, V., Voisset, M., 2011. Rare earth elements in cold seep carbonates from the Niger delta. Chemical Geology 286, 196-206. https://doi.org/10.1016/j.chemgeo.2011.05.001.

Rothwell, R.G., 2006. New Techniques in Sediment Core Analysis. Geological Society, London, Special Publications 267, 65-77. https://doi.org/10.1144/GSL.SP.2006.267.01.01.

Rouby, D., Nalpas T., Jermannaud P., Robin C., Guillocheau F., Raillard S., 2011. Gravity driven deformation controlled by the migration of the delta front: The Plio-Pleistocene of the Eastern Niger Delta. Tectonophysics 513, 54-67. https://doi.org/10.1130/GEOSO1426.1.

Ruffine, L., Caprais, J.C., Bayon, G., Riboulot, V., Donval, J.P., Etoubleau, J., Birot, D., Pignet, P., Rongemaille, E., Chazallon, B., Grimaud, S., Adamy, J., Charlou, J.L., Voisset, M., 2013. Investigation on the geochemical dynamics of a hydrate-bearing pockmark in the Niger Delta. Marine and Petroleum Geology 43, 297-309. https://doi.org/10.1016/j.marpetgeo.2013.01.008.

Saugy, L., Eyer, J.A., 2003. Fifty years of exploration in the Niger Delta (West Africa). In: Halbouty, M.T. (Ed.), Giant Oil and Gas Fields of the Decade 1990-1999. American Association of Petroleum Geologists memoir 78, 211-226. https://doi.org/10.1306/M78834C12.

Schmidt, C., Gupta, S., Rüpke, L., Burwicz-Galerne, E., Hartz, E.H., 2022. Sedimentation-driven cyclic rebuilding of gas hydrates. Marine and Petroleum Geology 140, 105628. doi:10.1016/j.marpetgeo.2022.105628.

Serov, P., Vadakkepuliyambatta, S., Mienert, J., Patton, H., Portnov, A., Silyakova, A., Panieri, G., Carroll, M.L., Carroll, J., Andreassen, K., Hubbard, A., 2017. Postglacial response of Arctic Ocean gas hydrates to climatic amelioration. Earth, Atmospheric, and Planetary Sciences 114, 24, 6215-6220. https://doi.org/10.1073/pnas.1619288114.

Shackleton, N.J., Berger, A., Peltier, W.R., 1990. An alternative astronomical calibration of the lower Pleistocene timescale based on ODP site 677. Transactions of the Royal Society of Edinburgh: Earth Sciences 81, 251-261. https://doi.org/10.1017/S0263593300020782.

Shakhova, N., Semiletov, I., Leifer, I., Sergienko, V., Salyuk, A., Kosmach, D., Chernykh, D., Stubbs, C., Nicolsky, D., Tumskoy, V., Gustafsson, Ö., 2014. Ebullition and storm-induced methane release from the East Siberian Arctic Shelf. Nature Geosciences 7, 64-70. https://doi.org/10.1038/ngeo2007.

Short, K.C., Stauble, A.J., 1967. Outline of geology of Niger delta. American Association of Petroleum Geologists Bull. 15, 761-779. https://doi.org/10.1306/5D25C0CF-16C1-11D7-8645000102C1865D

Stacher, P., 1995. Present understanding of the Niger Delta hydrocarbon habitat. In: Oti, M.N., Postma, G., (Eds.), Geology of deltas, 257-267.

Stewart, S.A., Davies, R.J., 2006. Structure and emplacement of mud volcano systems in the South Caspian Basin. American Association of Petroleum Geologists Bull. 90, 771-786. https://doi.org/10.1306/11220505045.

Stott, L., Davy, B., Shao, J., Coffin, R., Pecher, I., Neil, H., Rose, P., Bialas, J., 2019. CO2 release from pockmarks on the Chatham rise-bounty trough at the glacial termination. Paleoceanography and paleoclimatology 34, 1726-1743. https://doi.org/10.1029/2019pa003674.

Suess, 2014. Marine cold seeps and their manifestations: geological control, biogeochemical criteria and environmental conditions. International Journal Of Earth Sciences 103, 1889-1916. https://doi.org/10.1007/s00531-014-1010-0.

Sultan, N., Voisset, M., Marsset, T., Vernant, A.M., Cauquil, E., Colliat, J.L., Curinier, V., 2007. Detection of free gas and gas hydrate based on 3D seismic data and cone penetration testing: an example from the Nigerian Continental Slope. Marine Geology 240, 235-255. https://doi.org/10.1016/j.margeo.2007.02.012.

Sultan, N., Marsset, B., Ker, S., Marsset, T., Voisset, M., Vernant, A.M., Bayon, G., Cauquil, E., Adamy, J., Colliat, J.L., Drapeau, D., 2010. Hydrate dissolution as a potential mechanism for pockmark formation in the Niger delta. Journal of Geophysical Research 115, B08101. https://doi.org/10.1029/2010JB007453.

Sultan, N., Riboulot, V., Ker, S., Marsset, B., Geli, L., Tary, J.B., Klingelhoefer, F., Voisset, M., Lanfumey, V., Colliat, J.L., Adamy, J., Grimaud S., 2011. Dynamics of fault-fluid-hydrate system around a shale-cored anticline in deepwater Nigeria. Journal of Geophysical Research 116, B12110. https://doi.org/10.1029/2011JB008218.

Sultan, N., Bohrmann, G., Ruffine, L., Pape, T., Riboulot, V., Colliat, J.L., De Prunelé, A., Dennielou, B., Garziglia, S., Himmler, T., 2014. Pockmark formation and evolution in deep water Nigeria: rapid hydrate growth versus slow hydrate dissolution. Journal of Geophysical Research: Solid Earth 119, 2679-2694. https://doi.org/10.1002/2013JB010546.

Sultan, N., Garziglia, S., Ruffine, L., 2016. New insights into the transport processes controlling the sulfate-methane-transition-zone near methane vents. Scientific Reports 6, 26701. https://doi.org/10.1038/srep26701.

Sun, Q., Wu, S., Cartwright, J., Lüdmann, T., Yao, G., 2013. Focused fluid flow systems of the Zhongjiannan Basin and Guangle Uplift, South China Sea. Basin Research 23, 97-111. https://doi.org/10.1111/j.1365-2117.2012.00551.x.

Taleb, F., Garziglia, S., Sultan, N., 2018. Hydromechanical properties of gas hydrate-bearing fine sediments from in situ testing. Journal of Geophysical Research: Solid Earth 123, 9615-9634. https://doi.org/10.1029/2018JB015824.

Taleb, F., Lemaire, M., Garziglia, S., Marsset, T., Sultan, N., 2020. Seafloor depressions on the Nigerian margin: Seabed morphology and sub-seabed hydrate distribution. Marine and Petroleum Geology 114, 104175. https://doi.org/10.1016/j.marpetgeo.2019.104175.

Talukder, A.R., 2012. Review of submarine cold seep plumbing systems: leakage to seepage and venting. Terra Nova 24, 255-272. https://doi.org/10.1111/j.1365-3121.2012.01066.x.

Trehu, A.M., Flemings, P.B., Bangs, N.L., Chevallier, J., Gracia, E., Johnson, J.E., Liu, C.S., Liu, X.L., Riedel, M., Torres, M.E., 2004. Feeding methane vents and gas hydrate deposits at south Hydrate Ridge. Geophysical Research Letters 31, L23310. https://doi.org/10.1029/2004GL021286.

Tuttle, M.L.W., Charpentier, R.R., Brownfield, M.E., 1999. The Niger Delta Petroleum System: Niger Delta Province, Nigeria, Cameroon, and Equatorial Guinea, Africa. Open-File Report 99-50-H. U.S. Department of the interior U.S. Geological Survey. https://doi.org/10.3133/OFR9950H.

Voisset, M., 2003. NERIS 1 cruise, RV Le Suroît. https://doi.org/10.17600/3020010.

Voisset, M., 2004. NERIS 2 cruise, RV L'Atalante. https://doi.org/10.17600/4010010.

Waage, M., Portnov, A., Serov, P., Bünz, S., Waghorn, K.A., Vadakkepuliyambatta, S., Miniert., J., Andreassen, K., 2019. Geological Controls on Fluid Flow and Gas Hydrate Pingo Development on the Barents Sea Margin. Geochemistry, Geophysics, Geosystems 20, 630-650. https://doi.org/10.1029/2018GC007930.

Wallmann, K., Aloisi, G., Haeckel, M., Obzhirov, A., Pavlova, G., Tishchenko, P., 2006. Kinetics of organic matter degradation, microbial methane generation, and gas hydrate formation in anoxic marine sediments. Geochimica et Cosmochimica Acta 70, 3905-3927. https://doi.org/10.1016/j.gca.2006.06.003.

Weldeab, S., Lea, D.W., Schneider, R.R., Andersen, N., 2007. 155,000 years of West African monsoon and ocean thermal evolution. Science 316, 1303-1307. https://doi.org/10.1126/science.1140461.

Weldeab, S., Frank, M., Stichel, T., Haley, B., Sangen, M., 2011. Spatio-temporal evolution of the West African monsoon during the last deglaciation. Geophysical Research Letters 38, L13703. https://doi.org/10.1029/2011GL047805.

Wei, J., Pape, T., Sultan, N., Colliat, J.-L., Himmler, T., Ruffine, L., et al., 2015. Gas hydrate distributions in sediments of pockmarks from the Nigerian margin – Results and interpretation from shallow drilling. Marine and Petroleum Geology 59, 359-370. https://doi.org/10.1016/j.marpetgeo.2014.09.013.

Whiteman, A.J., 1982. Nigeria: Its Petroleum Geology, Resources and Potential. Graham and Trotman, London, 394 pp. https://doi.org/10.1007/978-94-009-7361-9.

Wu, S., Bally, A.W., 2000. Slope tectonics-comparisons and contrasts of structural styles of salt and shale tectonics of the northern Gulf of Mexico with shale tectonics of offshore Nigeria in Gulf of Guinea. In: Mohriak, W., Talwani, M. (Eds.), Atlantic Rifts and Continental Margins. American Geophysical Union Geophysical Monograph Series 115, 151-172. https://doi.org/10.1029/GM115p0151.

Wu, J. E., McClay, K., Frankowicz, E., 2015. Niger Delta gravity-driven deformation above the relict Chain and Charcot fracture zones, Gulf of Guinea: Insights from analogue models. Marine and Petroleum Geology 65, 43-62. https://doi.org/10.1016/j.marpetgeo.2015.03.008.

Xiao, H., Suppe, J., 1992. Origin of rollover: American Association of Petroleum Geologists Bull. 76, 509-229.

Xu, W., Germanovich, L.N., 2006. Excess pore pressure resulting from methane hydrate dissociation in marine sediments: a theoretical approach. Journal of Geophysical Research 111, B01104. https://doi.org/10.1029/2004JB003600.

Yahaha-Joe, U., Okikiade, F., Ghosh, D.P., 2000. Geohazard analysis in deepwater Nigeria. OTC-11924-MS, Houston, Texas. https://doi.org/10.4043/11924-MS.

Yusifov, M., Rabinowitz, P.D., 2004. Classification of mud volcanoes in the South Caspian Basin, offshore Azerbaijan. Marine and Petroleum Geology 21, 965-975. ISSN 0264-8172. https://doi.org/10.1016/j.marpetgeo.2004.06.002.

Zabel, M., Schneider, R.R., Wagner, T., Adegbie, A.T., de Vries, U., Kolonic, S., 2001. Late Quaternary Climate Changes in Central Africa as Inferred from terrigenous input to the Niger Fan. Quaternary Research 56, 207-217. https://doi.org/10.1006/qres.2001.2261.

Zhao, X., Qi, K., Liu, L., Gong, C., McCaffrey, W.D., 2018. Development of a partially-avulsed submarine channel on the Niger Delta continental slope: Architecture and controlling factors. Marine and Petroleum Geology 95, 30-49. https://doi.org/10.1016/j.marpetgeo.2018.04.015.